2020/5

We are pleased to announce the organization of

ec-siliconf2
THE 2ND EUROPEAN CONFERENCE
ON SILICON AND SILICA BASED MATERIALS
to be held in Hotel Palota in Miskolc-Lillafüred, Hungary, in October 4-8, 2021

The **ec-siliconf2** conference will be held in the wonderful palace of **Hotel Palota** in the exceptionally beautiful environment of **Beech Mountain** in **Miskolc-Lillafüred** in **Hungary**. In 2019 in the previous conference scientists had participated from **21** countries of **Asia, Europe, North- and South America** and **Africa**.

THE CONFERENCE SESSIONS

SESSION 1: Silicon and silica in inorganic and molecular chemistry
SESSION 2: Metallic silicon and silicon as an alloying agent
SESSION 3: Silicon (Si) and silica (SiO2) in medicine, therapy and health
SESSION 4: Silicon in micro and nanoelectronics and devices
SESSION 5: Silicon and silica in functional materials
SESSION 6: Silicon and silica in polymers
SESSION 7: Silicon and silica in ceramics and composites
SESSION 8: Silicon and silica in construction materials and glass
SESSION 9: Silicon and silica in biological systems and technologies
SESSION 10: Silicon and silica in smart materials and technologies
SESSION 11: Silicon and silica in minerals and rocks
SESSION 12: Testing and characterization methods, tools and errors
SESSION 13: Other results in research and development of silicon and silica and materials contain of them
SESSION 14: Other results in processing and application of silicon and silica and materials contain of them
SESSION 15: Miscellaneous in silicon and silica materials science

Registration abstract submission, and further information are available in:
www.ec-siliconf.eu

építőanyag

Journal of Silicate Based and Composite Materials

2020/5

TARTALOM

CONTENT

A finomkerámia-, üveg-, cement-, mész-, beton-, tégla- és cserép-, kő- és kavics-, tűzállóanyag-, szigetelőanyag-iparágak szakmai lapja
Scientific journal of ceramics, glass, cement, concrete, clay products, stone and gravel, insulating and fireproof materials and composites

Vol. 72, No. 5

Natural titanium dioxide nanotubes

Aleksei V. PONARYADOV ▪ Institute of Geology, Komi Science Center,
Ural Branch of the Russian Academy of Sciences, Russian Federation ▪ avponaryadov@geo.komisc.ru

Olga B. KOTOVA ▪ Institute of Geology, Komi Science Center,
Ural Branch of the Russian Academy of Sciences, Russian Federation ▪ kotova@geo.komisc.ru

Mohammed TIHTIH ▪ Institute of Ceramics and Polymer Engineering,
University of Miskolc, Hungary ▪ medtihtih@gmail.com

Shiyong SUN ▪ Institute of Non-metallic Minerals, Department of Geological Engineering,
School of Environment and Resource, Southwest University of Science and Technology,
People's Republic of China ▪ shiysun@163.com

Aleksei V. PONARYADOV
is a Researcher of Laboratory of Technology of Mineral Raw, Institute of Geology, Komi Science Center, Ural Branch of the Russian Academy of Sciences. Author and co-author of more than 30 scientific articles. Russian Mineralogical Society.

Olga B. KOTOVA
is Dr.Sc., Head of Laboratory of Technology of Mineral Raw, Institute of Geology, Komi Science Center, Ural Branch of the Russian Academy of Sciences. Author and co-author of 4 patents and more than 200 scientific articles. President of ICAM-2019. The member of Science Council of Russian Mineralogical Society.

Mohammed TIHTIH
Is a lecturer in the Sidi Mohamed Ben abdellah University, Morocco, he graduated from Faculty of sciences Dhar El Mahraz, Fez, Morocco, Department of Physics, for the time being, he is a PhD student in the University of Miskolc, Institute of Ceramics and Polymer Engineering, under supervision of Prof. L. A. Gömze

Shiyong SUN
is a Professor and Head of School of Environment and Resource at the Southwest University of Science and Technology. Author and co-author of more than 100 scientific articles.

Abstract

One-dimensional nanosized structures based on titanium dioxide are a desirable product because of their physical and chemical properties. The article considers production of titanium dioxide nanotubes based on ilmenite-leucoxene ores and products of their processing. Titanium dioxide nanotubes were synthesized by hydrothermal treatment in an alkaline solution from a gravity concentrate of ilmenite-leucoxene ore from the Pizhemskoe deposit. In the samples we found phases of quartz and sodium titanate $Na_xH_{2-x}Ti_3O_7$. Nanostructuring results in increasing specific surface area and decreasing band gap. We evaluated effectiveness of synthesized samples in the photocatalytic decomposition of organic pollutants in aqueous solutions. We showed that they were not inferior to commercial analogues by their effectiveness.

Keywords: functional materials, titanium dioxide, nanotubes, ilmenite-leucoxene ore, photocatalysis

Kulcsszavak: funkcionális anyagok, titán-dioxid, nanocsövek, ilmenit-leucoxén érc, fotokatalízis

1. Introduction

Composite and other advanced materials can obtain properties of the initial raw [1-3]. Titanium dioxide-based materials attract attention of scientists and engineers due to a set of physical and chemical characteristics (for example, high Ti-O bond strength, low redox potentials).

Due to optical properties, it was most widely used in the paint and varnish industry and in the production of pigments. Also, the objects of close attention of researchers are sensor, adsorption, optical, electrical and catalytic properties of TiO_2. The photocatalytic properties of TiO_2 are also a subject of increased interest, which allows increasing efficiency of technological processes for the photocatalytic purification of water and air from toxic organic impurities. Chemical and biological inertness allows creating anticorrosion coatings, matrices for the disposal of radioactive waste, and implants [4–6].

The trend of recent decades has been a directed change of the physical and chemical properties of various materials at the nanoscale [7–11]. Particular attention is drawn to the production of nanostructured TiO_2 particles [12–18], which is associated with the physical and chemical properties of nanoparticles other than macroparticles, such as gravity forces, chemical, electromagnetic, rheological, or optical. The most of published works on the synthesis of nanostructured TiO_2 particles are devoted to synthetic raw materials.

Practically no attention is paid to producing titanium nanodioxide from natural raw – in particular, from a gravity concentrate of titanium ores. When developing new or adapting existing methods, a complex nature of natural raw should be considered. Thus, in ilmenite-leucoxene ores (Pizhemskoe titanium deposit), the main source of valuable components is ilmenite and its alteration products (leucoxene), which are represented by polymineral microaggregates with complex morphostructural features, in which quartz grains occupy up to 30 % (on average). Therefore, during producing nanostructured titanium dioxide directly from the gravity concentrate of ilmenite-leucoxene ore, we should consider possibility of their removal or dissolution.

The aim of this work is to study synthesis of nanostructures based on natural titanium raw – leucoxene ore, and their physical-chemical properties.

2. Materials and experiments

2.1 Materials

We used samples of gravity concentrate of ilmenite-leucoxene ore from the Pizhemskoe deposit, Russia (hereinafter – LC). At hydrothermal synthesis, NaOH (purity ≥98 %), HCl (≥ 85%, NevaReaktiv) were used without additional purification. For the preparation of working solutions, deionized water was used.

2.2 Synthesis of nanostructures

In a typical preparation 0.8 g of starting ore (reduced size) was placed in 100 ml autoclave, where 80 ml of 10 M NaOH solution were added. The autoclave was kept at 110 °C during 24 h (temperature sensor was mounted on the stove, not inside the autoclave). After the hydrothermal reaction the autoclave was cooled to room temperature, and the resulting flaky precipitate was washed successively by distilled water and solution of hydrochloric acid (0.1 M) until neutral pH (6.5-7). The washed samples were dried in the oven at 90 °C for 12 hours.

2.3 Samples characterization

The morphology, phase and chemical composition of the starting ore and as-synthesized samples were studied using a complex of modern analytical equipment in Institute of Geology Komi SC

UB RAS and Southwest University of Science and Technology. Nanotubes were visualized by scanning electron microscopy (TESCAN Vega 3; SIRMA 300). The crystalline structures of the initial ore and synthesized samples were analyzed by diffractometer (Shimadzu XRD-6000), the material composition was studied by X-ray fluorescence (XRF Shimadzu-1800).

The photocatalytic activity of the samples was studied using a test reaction of decomposition of trichlorophenol in Hereaus circular reactor of a volume of 350 cm³. Vertically to the reactor axis the TQ150 Z2 mercury lamp (150 W, 352–540 nm) was located. The control solutions were analyzed by liquid chromatography (Hypersil C18 reverse phase HPLC column). The solvent was a solution of acetonnitrile in water in a ratio of 3:2. The solvent flow was 0.5 ml/min.

3. Results and discussion

3.1 Mineralogical analysis

The titanium minerals in LC sample are represented by ilmenite, rutile, anatase. Leucoxene, an aggregate of rutile and quartz, is represented by grains of yellow and slightly pinkish color and elongated along one of the axes [19].

The phase analysis showed that LC is basically a mixture of two phases: rutile and quartz (*Fig. 1, A*). The peaks are clear, indicating a high degree of perfection of rutile. Weak reflexes of ilmenite and anatase are present.

LC is represented by rounded isometric and oval flattened aggregates of needle microcrystals of rutile and quartz with relics of pseudorutile (*Fig. 1, B-C*). Rutile microcrystals form a sagenite lattice of rutile twins, fused at an angle of 60°. There are also areas of development of anatase crystallites, which are a homogeneous mass. The quartz grains have clear crystallographic forms, the surface is porous.
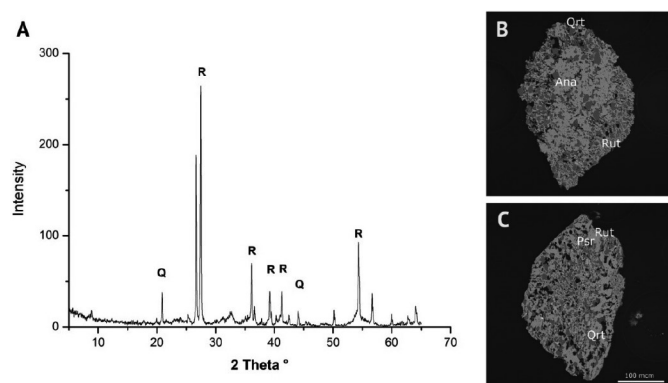
1. ábra A - LC diffrakciós minta (Q - kvarc, R - rutil); B, C - leucoxén szemcsék anatáz zárványokkal: Rut - rutile, Ana - anatase, Psr - pseudorutile, Qrt - quartz. Az ásványi fázisokat EBSD határozta meg.

Fig. 1 A – LC diffraction pattern (Q – quartz, R – rutile); B, C – leucoxene grains with anatase inclusions: Rut – rutile, Ana – anatase, Psr – pseudorutile, Qrt – quartz. Mineral phases determined by EBSD.

Iron in LC grains is concentrated inside aggregates and associated with pseudorutile relics with clear boundaries. Smaller sections of pseudorutile — residues of the primary mineral — are observed along the perimeter of relics. The volume fraction of quartz and aluminosilicate phases is from 18 to 38 %; average value of 28 %.

Thus, LC grains are a polymineral aggregate, the sizes of individual phases from a few micrometers to 100 micrometers. Quartz cannot be reliably separated by physical methods.

3.2 Nanostructured titanium dioxide

The synthesized sample, hereinafter NT, (*Fig. 2*) is a mixture of two phases: quartz and hydrated sodium titanate ($Na_xH_{2-x}Ti_3O_7$). Chemical composition (wt.%): TiO_2 – 74.68, SiO_2 – 12.64, Fe_2O_3 – 5.44, Al_2O_3 – 4.71, Na_2O – 0.14, K_2O – 0.93, MnO – 0.64, CaO – 0.12, MgO – 0.25, P_2O_5 – 0.09, ZrO_2 – 0.08, NbO – 0.14.

The formation of titanium dioxide nanotubes proceeds in several stages: a gradual dissolution of raw is accompanied by epitaxial growth of layered sodium titanate nanosheets → nanolayer delamination → twisting of nanosheets into tubes → nanotube growth along X axis → exchange of sodium ions by protons during washing and separation of nanotubes from each other. When treated with alkali, the crystal lattice of the initial rutile turns into an amorphous product; after treatment with distilled water and a solution of hydrochloric acid, titanium dioxide nanotubes are formed [20]. According to [13], nanotubes consist of titanate layers, the composition of which depends on the synthesis conditions (temperature, processing time, ratio of liquid and solid phases). Tubular twisting of atomic layers is accompanied by a noticeable expansion of the shape of the peaks. *Fig. 2A* shows indices of planes corresponding to the peaks of the diffraction pattern. The reflection characteristic of titanium dioxide nanotubes in the region $2\theta = 10°$ can be attributed to $H_2Ti_3O_7$ or $Na_xH_{2-x}Ti_3O_7$ crystals [21]. Reflexes (200) with an interlayer distance 0.96 nm correspond to the distance between two adjacent TiO_6 octahedra that form the walls of the nanotubes.

Fig. 2 shows an electron microscopic image of the synthesized TiO_2 nanotubes. The channels inside the obtained nanotubes are clearly visible. The resolution of a scanning electron microscope allows estimating their outer diameter (70–100 nm).

Nanostructural rearrangement results in increasing specific surface and changing band gap. Measurements by low temperature nitrogen adsorption (BET) are given in *Table 1*.
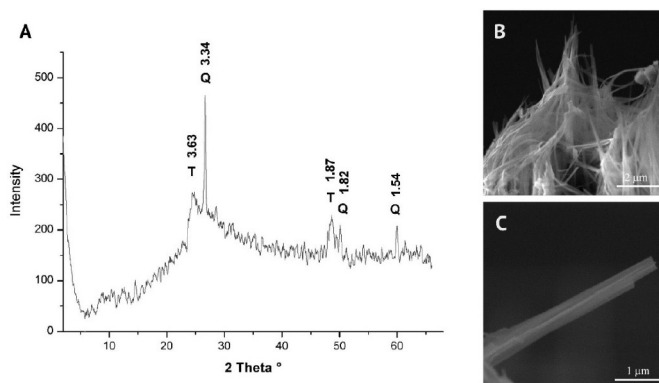
2. ábra A - NT diffrakciós mintázat (Q-kvarc, T-nátrium-titanát); B, C - nanocsövek SEM képei

Fig. 2 A – NT diffraction pattern (Q – quartz, T – sodium titanate); B, C – SEM images of nanotubes

Sample	Band gap (eV)	Specific surface area, average values (m²/g)
Anatase	3.1	80
LC	2.8	13
NT	2.4	230

1. táblázat   Sávrés és fajlagos felület
Table 1   Band gap and specific surface area

The band gap was calculated by reflection spectra in the visible region based on the relationship of the adsorption coefficient α with the absorbed photon energy *hv* [13]:

$$\alpha = \frac{B_i \left(hv - \Delta E_g \right)^2}{hv},$$

where B_i – adsorption constant for indirect i-transitions. Structural rearrangement at the nanoscale level — the formation of titanium dioxide nanotubes — results in decreasing band gap: anatase — 3.1, LC — 2.8, NT — 2.4 eV.

The change in physical and chemical properties allows considering the obtained nanostructured samples as promising photocatalysts and using them in water treatment systems.

3.3 Study of photocatalytic properties

The photocatalytic activity of the samples was studied by a trichlorophenol decomposition reaction test. Commercially available titanium dioxide powders Aeroxide Degussa P25 and Anatase (Aldrich), widely used as an active catalyst in water treatment systems, were used as composites. According to the manufacturer, P25 is a weakly aggregated powder, the surface area is 50 m²/g, the phase composition – 25 % rutile and 75 %. Anatase characteristics are given in *Table 1*.

The kinetics of the heterogeneous photooxidation reaction in liquid media in the presence of a catalyst is described by the Langmuir – Hinshelwood model [22]. In this model, the reaction rate r is presented as a function of the degree of adsorbate coverage of active surface adsorption centers, which is assumed to be equal to the equilibrium adsorption θ associated with the concentration of adsorbate C through the equation of the Langmuir adsorption isotherm Eq. (1). The expression for the reaction rate should also contain other parameters, the consideration of which is possible only when constructing an adsorption model and adopting some simplifications. In particular, the size of the catalyst and the rate of transfer of active oxygen can be neglected. However, in this case as well, the process remains rather complicated for modeling, since the adsorption of trichlorophenol and decomposition products proceeds in parallel. Nevertheless, a fairly simple equation can be used if we consider only the process of photocatalytic decomposition of trichlorophenol (neglecting post-absorption). If we assume that the reaction rate between the adsorbate and the active Bronsted and Lewis surface centers (h⁺ and e⁻) can be represented as kθ, and the recombination rate of electron-hole pairs h⁺/e⁻ (kr) is quite high (kr>>kθ), then

$$r = -\frac{dC}{dt} = \frac{I\Phi}{k_r} k\theta = \frac{I\Phi}{k_r} k \frac{nKC}{1+KC} = k_{app} \frac{C}{1+KC} \qquad (1)$$

In the above equation, I – intensity of the incident radiation, Φ – degree of coverage of the surface of the sample by adsorbate,

n – surface concentration of active centers, K – equilibrium adsorption coefficient. If the concentration of adsorbate C is small, then Eq. (2) can be represented as:

$$r = k_{app} C \qquad (2)$$

In the integrated form, the last two equations, respectively

$$\ln\left(\frac{C_0}{C}\right) + K\left(C_0 - C\right) = k_{app} t \qquad (3)$$

and

$$\ln\left(\frac{C_0}{C}\right) = k_{app} t \qquad (4)$$

In this case, for the decomposition reaction of trichlorophenol, taking into account Eq. (4), the time dependence is linear, and the slope gives the constant k_{app}. Graphs of time dependence for the studied samples are presented in *Fig. 3*.
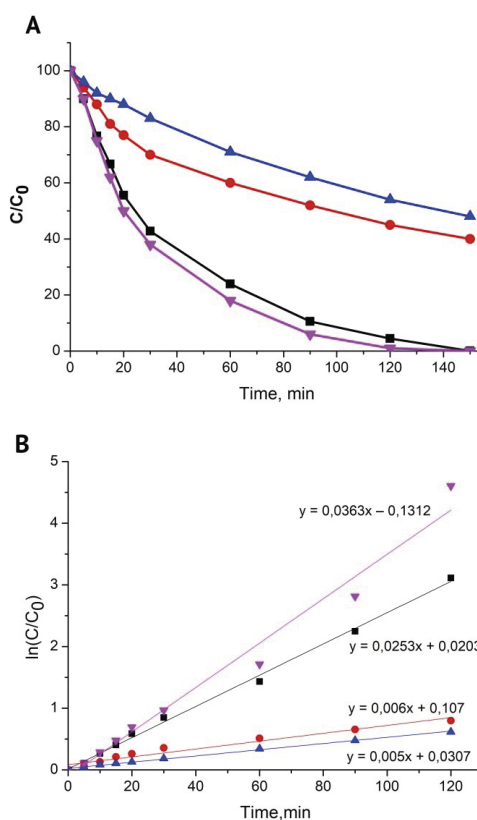
3. ábra   A - Triklór-fenol lebomlási görbék vizes közegben; B - a reakcióállandók kiszámításához (■ - Degussa P25, ● - anatáz, ▲ - LC, ▼ - NT)
Fig. 3   A – Trichlorophenol degradation curves in an aqueous medium; B – for calculation of reaction constants (■ – Degussa P25, ● – anatase, ▲ – LC, ▼ – NT)

Linear approximation is applicable only in a certain time interval. This can be explained by the fact that post-absorption processes, i.e. interaction of the surface of the samples with intermediate products of the decomposition reaction of trichlorophenol were not taken into account. When using the Langmuir-Hinshelwood model, it is assumed that the rate of adsorption on the surface significantly exceeds the rate of the reaction proceeding at active surface centers, i.e. the liquid phase and the surface of the sample are constantly in a state of adsorption equilibrium. Although the adsorption and decomposition reactions on the surface proceed

simultaneously, most likely, they do not determine the reaction rate. In the initial period of time (0–10 min), trichlorophenol is adsorbed on the surface of the sample and the reaction rate increases. Upon reaching complete coverage of the surface with the adsorbate, the reaction rate is maximum and does not change further. At this point, the decomposition reaction of trichlorophenol will be of zero order.

Based on the obtained data, the values of the reaction constants were calculated (*Fig. 3 B*): 0.005 for LC, 0.006 for anatase, 0.025 for Degussa P25 and 0.036 for NT.

4. Conclusions

We have synthesized titanium dioxide nanotubes by the hydrothermal method. Affordable natural raw material — a gravity concentrate of titanium ore from the Pizhemskoe deposit — has been used as an initial material. The synthesized titanium dioxide nanotubes have an external diameter of 70–100 nm. The synthesized material – TiO_2 nanotubes have a developed surface, which gives it good sorption qualities.

We have studied dependence of the kinetics of photoinduced decomposition of trichlorophenol in aqueous solutions in the presence of various types of catalysts based on titanium dioxide: commercially available Degussa P25 and anatase (Aldrich), leucoxene concentrate (Pizhemskoe deposit), titanium dioxide nanotubes. The reaction constants of photoinduced decomposition of trichlorophenol are calculated. We have shown that titanium dioxide nanotubes are not inferior in characteristics to commercial analogues currently used as the basis for catalysts.

Acknowledgements

References
[1] T.N., Shchemelinina – A. L., Gömze – O. B., Kotova – J.E.F.M., Ibrahim – D. A., Shushkov – M., Harja – G. V., Ignatiev – E. M., Anchugova (2019): Clay- and zeolite-based biogeosorbents: modelling and properties *Építőanyag–JSBCM*, Vol. 71, No.4, pp.131–137. p. https://doi.org/10.14382/epitoanyag-jsbcm.2019.23
[2] T., Shchemelinina – O., Kotova – M., Harja – E., Anchugova (2019): Biogeosorbents for solving ecological problems // *IOP Conf. Series: Materials Science and Engineering* Vol. 613, 012042 https://doi.org/10.1088/1757-899X/613/1/012042
[3] E., Kurovics – O.B., Kotova – A.L., Gömze – D.A., Shushkov – G.V., Ignatiev – P. A., Sitnikov – Y. I., Ryabkov – I. N.,Vaseneva – L. N., Gömze (2019): Preparation of particle-reinforced mullite composite ceramic materials using kaolin and IG-017 bio-origin additives *Építőanyag–JSBCM*, Vol. 71, No.4, pp.114–119. https://doi.org/10.14382/epitoanyag-jsbcm.2019.20
[4] K. D., Kumar – G. P., Kumar – K. S., Reddy (2015): Rapid Microwave Synthesis of Reduced Graphene Oxide-supported TiO_2 Nanostructures as High Performance Photocatalyst. *Materials Today*. No. 2, pp. 3736–3742.
[5] W., Zhang – C. R., Ou – Z.G., Yuan (2017): Precipitation and growth behaviour of metatitanic acid particles from titanium sulfate solution. *Powder Technology*, No.315, pp. 31–36.
[6] O. B., Kotova – I. L., Shabalin – D. A., Shushkov – A. V., Ponaryadov (2015): Sorbents based on mineral and industrial materials for radioactive wastes immobilization. *Vestnik of Insitute of Geology*, Vol. 2, pp. 32-34.
[7] J. E. F. M., Ibrahim – A. L., Gömze – O. B., Kotova – T. N., Shchemelinina – D. A., Shushkov – G.V., Ignatiev – E. M., Anchugova (2019): The influence of composition, microstructure and firing temperature on the density, porosity, and shrinkage of new zeolite-alumina composite material. *Építőanyag–JSBCM*, Vol. 71, No.4, pp.120–124. https://doi.org/10.14382/epitoanyag-jsbcm.2019.21
[8] D. P., Penaloza Jr. (2019): Enhanced mechanical, thermal and barrier properties of clay-based polymer nanocomposite systems. *Építőanyag–JSBCM* Vol. 71 No. 3 pp. 74–79. https://doi.org/10.14382/epitoanyag-jsbcm.2019.13
[9] O. B., Kotova – D. A., Shushkov – A. L., Gömze – E., Kurovics – G. V., Ignatiev – P. A., Sitnikov – Y. I., Ryabkov – I. N., Vaseneva (2019): Composite materials based on zeolite-montmorillonite rocks and aluminosilicate wastes. *Építőanyag–JSBCM*, Vol. 71, No.4, pp. 125–130. https://doi.org/10.14382/epitoanyag-jsbcm.2019.22
[10] F., Hu – Y., Wen – K. C., Chan – T. M., Yue – Y. Z., Zhou – S. L., Zhu – X. J., Yang (2015): Synthesis of self-detached nanoporous titanium-based metal oxide. *Journal of Solid State Chemistry* Vol. 229, Pages 78-86 https://doi.org/10.1016/j.jssc.2015.05.021
[11] S., lIssar – A. K., Mahapatro (2019): Hydrothermally grown rutile titanium dioxide nanostructures with various morphologies. *Materials Science in Semiconductor Processing*, Vol. 104, 104676. https://doi.org/10.1016/j.mssp.2019.104676
[12] O. B., Kotova – M.,Harja – L. N., Kotov – A. V., Ponaryadov (2018): Titanium minerals as prototypes of functional materials with pronounced electromagnetic properties. *Vestnik IG Komi SC UB RAS*. No. 4. C. 34–39.
[13] L. H., Huang – C., Sun – Y. L., Liu (2007) Pt/N-codoped TiO_2 nanotubes and its photocatalytic activity under visible light. *Applied Surface Science*, Vol. 253, pp. 7029–7035.
[14] H.-L., Kuo – C.-Y., Kuo – C.-H., Liu – J.-H., Chao – C.-H., Lin (2007): A highly active bi-crystalline photocatalyst consisting of TiO_2 (B) nanotube and anatase particle for producing H2 gas from neat ethanol. *Catalysis Letters*, Vol. 113. P. 7–12.
[15] T. W. P., Seadira – G., Sadanandam – T., Ntho – C. M., Masuku – M. S., Scurrel (2018): Preparation and characterization of metals supported on nanostructured TiO_2 hollow spheres for production of hydrogen via photocatalytic reforming of glycerol. *Applied Catalysis B: Environmental*, Vol.222, pp.133-145
[16] N., Wang – X., Li – Y., Wang – X., Quan – G., Chen (2009): Evaluation of bias potential enhanced photocatalytic degradation of 4-chlorophenol with TiO_2 nanotube fabricated by anodic oxidation method. *Chemical Engineering Journal*, Vol. 146, pp. 30–35.
[17] Duduman C. N., – Gómez de Salazar y Caso de Los CobosJ. Harja M., – Barrena Pérez M. I., Gómez de Castro C., Lutic D., Kotova O., Cretescu I. (2018): Preparation and characterisation of nanocomposite materials based on TiO_2-Ag for environmental applications. *Environmental Engineering and Management Journal*. Vol.17, No. 4, pp. 2813-2821.
[18] O., Kotova – E., Ozhogina – A., Ponaryadov – I., Golubeva (2016): Titanium minerals for new materials. *IOP Conf. Series: Materials Science and Engineering*, 012025 https://doi.org/10.1088/1757-899X/123/1/012025
[19] A. V., Ponaryadov (2017) Mineralogical and technological features of ilmenite-leucoxene ores of Pizhemskoe deposit, Middle Timan. *Vestnik of the Institute of Geology, Komi SC UB RAS*. No. 1. pp. 29–36. https://doi.org/10.19110/2221-1381-2017-1-29-36 (in Russian)
[20] O. B., Kotova – A. V., Ponaryadov – L. A., Gömze (2016): Hydrothermal synthesis of TiO_2 nanotubes from concentrate of titanium ore Pizhemskoe deposit (Russia). *Vestnik IG Komi SC UB RAS*, No.1, pp. 34–36.
[21] Th., Streethawong – Y., Suzuki – S., Yoshikawa (2005): Synthesis, characterization, and photocatalytic activity for hydrogen evolution of nanocrystalline mesoporous titania prepared by surfactant-assisted templating sol–gel process. *Journal of Solid State Chemistry*, Vol. 178, pp. 329–338.
[22] Alaoui, O. Tahiri – Nguyen, Q. T. – Mbareck, C. – Rhlalou, T. (2009): Elaboration and study of poly (vinylidene fluoride)–anatase TiO_2 composite membranes in photocatalytic degradation of dyes, *Applied Catalysis A General* Vol. 358, pp. 13–20.

Analcime-bearing rocks as advanced sorbents

Dmitry A. Shushkov ▪ Institute of Geology, FRC Komi Science Center,
Ural Branch of the Russian Academy of Sciences, Russian Federation ▪ dashushkov@geo.komisc.ru

Olga B. Kotova ▪ Institute of Geology, FRC Komi Science Center,
Ural Branch of the Russian Academy of Sciences, Russian Federation ▪ kotova@geo.komisc.ru

Jamal-Eldin F. M. Ibrahim ▪ Institute of Ceramics and Polymer Engineering,
University of Miskolc, Hungary ▪ jamalfadoul@gmail.com

Maria Harja ▪ Gheorghe Asachi Technical University of Iași,
Faculty of Chemical Engineering and Environmental Protection, Iași, Romania ▪ maria_harja06@yahoo.com

László A. Gömze ▪ Institute of Ceramics and Polymer Engineering,
University of Miskolc, Hungary ▪ femgomze@uni-miskolc.hu

Tatyana N. Shchemelinina ▪ Institute of Biology, FRC Komi Science Center,
Ural Branch of the Russian Academy of Sciences, Russian Federation ▪ tatyanakomi@mail.ru

Grigoriy V. Ignatiev ▪ Institute of Geology, FRC Komi Science Center,
Ural Branch of the Russian Academy of Sciences, Russian Federation ▪ ignatiev.grigoriy@gmail.com

Abstract

The rational use of water and soil resources and their effective purification are actual scientific problems for modern society. Inexpensive and effective natural sorbents, zeolites, are widely used to solve environmental problems and improve the safety of the use of water and soil resources. This article presents results of our study of the sorption properties of analcime-bearing rocks in the north-east of the European part of Russia. Experiments and analytical studies were carried out using modern analytical equipment. The high sorption activity of these rocks with respect to radioactive elements (uranium, radium, thorium) was established. The simulated biogeosorbents based on analcime-bearing rocks and target microorganisms exhibited high sorption and destructive properties to oil products and phenols, ensured preservation and increased the growth of *Chlorella vulgaris* microalgae cells under stress conditions: with increased salinity and exposure to organic pollutants.

Keywords: analcime-bearing rocks, zeolites, sorbents, biogeosorbents, radionuclides, phenol
Kulcsszavak: analcimet hordozó kőzetek, zeolitok, szorbensek, biogeoszorbensek, radionuklidok, fenol

Dmitry A. SHUSHKOV
Researcher of Laboratory of Technology of Mineral Raw, Institute of Geology, FRC Komi Science Center, Ural Branch of the Russian Academy of Sciences. Author and co-author of 2 patents and more than 40 scientific articles. Russian Mineralogical Society.

Olga B. KOTOVA
is professor and Head of Laboratory of Technology of Mineral Raw, Institute of Geology, FRC Komi Science Center, Ural Branch of the Russian Academy of Sciences. Author and co-author of 4 patents and more than 150 scientific articles. Vice-president of International Commission on Applied Mineralogy (IMA-ICAM). Member of Russian Mineralogical Society.

Jamal Eldin F. M. IBRAHIM
is a lecturer in the University of Bahri, Khartoum, Sudan, he graduated from University of Marmara, Istanbul, Turkey, Institute of Pure and Applied Sciences, Department of Metallurgical and Materials Engineering, for the time being, he is a PhD student in the University of Miskolc, Institute of Polymer and Ceramics Engineering, under supervision of Prof. L. A. Gömze.

Maria HARJA
Is an associate professor in Department of Chemical Engineering at "Gheorghe Asachi" Technical University of Iasi, Romania. She is author or co-author of over 160 scientific papers (59 ISI) and 17 books.

László A. GÖMZE
is establisher and professor of the Department of Ceramics and Silicate Engineering in the University of Miskolc, Hungary. He is author or co-author of 2 patents, 6 books and more than 300 scientific papers.

Tatyana N. SHCHEMELININA
is a researcher and head of research group at the Institute of Biology, FRC Komi Science Center, Ural Branch of the Russian Academy of Sciences. She is author or co-author of several scientific papers both in English and Russian languages.

Grigoriy V. IGNATIEV
Junior researcher of Laboratory of Chemistry of Mineral Raw, Institute of Geology, Komi Science Center, Ural Branch of the Russian Academy of Sciences. He actually continues his studies as PhD student.

1. Introduction

Zeolites are microporous framework aluminosilicates with high sorption and ion exchange capacities. They have sufficient mechanical strength, thermal, chemical and radiation resistance; contain non-toxic exchange cations (Na, K, Ca, Mg). Their physical and chemical properties largely depend on the type of zeolite and, accordingly, the features of its structure: channel and pore size, cavity volume, Si/Al ratio, composition and position of cations. The main applications of zeolites in industry are catalysis, gas separation, and ion exchange [1–7]. The advantages of natural zeolites over synthetic analogues are their low price, a wide occurrence in the world, availability for mining. Compared to activated carbon, which is widely used in sorption processes, zeolites are characterized by lower regeneration costs [8, 9].

Currently, more than 90 types of natural zeolites are known [10, 11]. Industrial clusters form clinoptilolite, mordenite, phillipsite, chabazite, stilbite, laumontite and analcime [3]. Analcime belongs to narrow-porous zeolites with a channel size 0.16×0.42 nm [12, 13].

In sedimentary rocks, analcime is associated with clay minerals, which are characterized by high sorption properties. Therefore, such rocks can be considered as sorption raw materials of mixed composition. Earlier studies of analcime-

bearing rocks have shown that they can be used in various fields of industry.

Some authors suggest using analcime as a raw material for aluminum [14–17]. The use of various kinds of influence (T, hv, etc.) demonstrate the promise of using analcime-bearing rocks as raw materials for aluminum. So, in [18] experiments were conducted on the extractability of aluminum under acid exposure. It was shown that from 4.7 to 50.8 % Al_2O_3 passes into the solution. The highest recoverability of Al_2O_3 was achieved by exposure to 3 % HCl for 72 hours and 10 % H_2SO_4 for 24 and 120 hours. More than 30 % was recovered by treatment with concentrated HCl for 48 hours and 5 % HCl for 24 and 120 hours. The quantity of Al_2O_3 in solution depends on the processing time, particle size, type of acid. Al_2O_3 concentrations have a complex pattern depending on these parameters. In [19–21], bauxites and aluminosilicates are considered as metal concentrators.

Many works are devoted to the use of zeolites and clays as functional materials (ceramics, sorbents, etc.). Thus, a short-term annealing of analcime-bearing rocks at temperatures 1050–1150 °C resulted in light porous materials with water absorption 3–7 % and bulk density 260–280 kg/m³, which can be used as heat-insulating materials. The authors [18] showed a technological scheme for producing ceramic material suitable for the production of facing tiles and some types of electrical ceramics. Other authors showed the increase in the strength characteristics and heat resistance by 20–25 % of the epoxy composite material after introduction of analcime-bearing rocks from 0.5 to 25 % (wt.) [22, 23]. The data indicated suitability of the use of raw materials in crop production, animal breeding, soil-ecological and agrochemical fields.

This paper presents data on the sorption activity of analcime-bearing rocks in relation to radionuclides (uranium, radium, thorium) and their ability to hold them; the efficiency of use in the treatment of drinking water and wastewater of enterprises is shown; sorption and destructive properties of analcime-bearing rocks and biogeosorbents based on them in relation to oil products and phenols are estimated.

2. Objects and methods of investigation

2.1 Objects

The object of the study was the analcime-bearing rocks from several occurrences at the northeast of the European part of Russia: Veslyana (sample 551), Veslyanskoe – 1 (sample 56403), Eshmesskoe (sample 1/83), Chernorechenskoe (sample 58603).

2.2 Methods

The surface morphology and composition of samples were studied by TESCAN VEGA 3 LMH scanning electron microscope with X-Max energy dispersion attachment, Oxford Instruments, with an accelerating voltage 20 kV. Accelerating voltage 5 kV was used to study microorganisms.

The chemical composition of the rocks was determined by silicate analysis for 12/14 components.

X-ray phase analysis was performed by Shimadzu XRD 6000 diffractometer (CuKα radiation, Ni filter, 30 kV, 30 mA). A powder sample was taken in the range 2–65° 2θ with rate 1 deg/min and a scan step 2θ 0.05°. The phase composition of the clay fraction was determined by X-ray diffraction of oriented and non-oriented samples subjected to standard diagnostic treatments.

The specific surface area, the volume of micro- and mesopores, the total pore volume of the initial untreated powder sample were determined by the method of low-temperature physical sorption of nitrogen using a surface area and pore size analyzer NOVA 1200e, Quantachrome at a temperature of –196 °C with preliminary degassing at 350 °C in vacuum within 2 hours.

The specific surface area of biogeosorbents (grain size 0.1–0.25 mm) was determined in two modes: without preliminary degassing and with degassing at 25 °C in vacuum for 2 hours. Degassing with heating above 25 °C was not carried out because the microorganisms were not able to survive. The specific surface area was calculated by BET method, the mesopore volume – by BJH method, the micropore volume by the Dubinin-Astakhov method.

2.3 Experiments on the sorption of radionuclides

Sorption was carried out under static conditions at room temperature and 1:10 solid to liquid ratio (3 g of sorbent and 30 ml of solution) from aqueous solutions of uranyl nitrate, radium chloride and thorium chloride, in which the radionuclides were represented by a natural mixture of isotopes. The initial concentration of radionuclides in the solution was: radium – $0.32 \cdot 10^{-10}$ g/ml, uranium – $0.8 \cdot 10^{-6}$ g/ml, thorium – $0.5 \cdot 10^{-6}$ g/ml. The concentrations of radionuclides in model solutions were higher than in natural water, which commonly contains between $n \times 10^{-8}$ and $n \times 10^{-5}$ g/L uranium; thorium content is typically less than $n \times 10^{-8}$ g/L, radium content ranges from $n \times 10^{-14}$ to $n \times 10^{-11}$ g/L [24]. The contact time of the phases – 24 hours, pH of the solution – 6. The acidity of the liquid phase was adjusted to a certain level by alkalization with a concentrated (13 mol/L) ammonium hydroxide solution. pH of the liquid phase was measured by a compact pH meter "Wissenschaftlich-TechnischeWerkstatne GmbH", Germany.

The determination of natural radionuclides in the filtrates was carried out according to generally accepted methods. The uranium content was determined by the luminescent method (sensitivity $2.0 \cdot 10^{-8}$ g/g) by the luminescence of NaF pearls, the luminescence intensity was determined by LUF-57 photometer. The determination of thorium was carried out photocolorimetrically with arsenazo III with the separation of impurities by KU-2 cation exchange resin, the sensitivity of the method – $1.0 \cdot 10^{-8}$ g/g. Radium was determined by the emanation method using Alpha-1 instrument, sensitivity $2.0 \cdot 10^{-12}$ g/g.

The absorption strength (or desorption) was evaluated by the content in the extracts obtained by sequential treatment of the sorbent enriched with radionuclides with distilled water, 1M solutions of ammonium acetate (CH_3COONH_4) and 1M hydrochloric acid (HCl).

2.4 Experiments on purification of domestic and wastewater of industrial enterprises

We carried out studies on purification of drinking water of the Vychegda river. During our studies we compared effect of various types of filter media: analcime-bearing rocks with a grain size of -3.0+1.0 mm and quartz sand, which is currently used at a local water treatment plant. Filtered water samples were taken every 3 hours for 36 hours. The color, turbidity, iron content and permanganate oxidation were determined in the obtained samples according to standard methods. The initial indicators of water were as follows: turbidity – 2.71 mg/dm³, chromacity – 21 degrees, iron (total) – 1.06 mg/dm³, permanganate oxidation – 3.0 mg/dm³.

We conducted experiments on purification of wastewater from a boot factory (Vylgort town). The filter column was filled with an analcime-bearing rocks and contaminated water was passed through it. The following parameters were determined in the filtered water: pH, suspended solids, turbidity, COD, ammonium, oil products, phosphates.

2.5 Modeling of biogeosorbents for destruction of oil products

The following organisms were used as oil destructing organisms: Biotrin [25]: *Pseudomonas yamanorum* VKM B-3033D bacteria [26]; *Rhodotorula glutinis* yeast, VKM Y-2998D [27]; microalgae *Chlorella vulgaris* Beijer. f. *globosa* V. Andr [28].

The bacteria biomass was accumulated on MPA medium: per 1000 ml of water – peptone – 20 g; NaCl – 3.0 g; KCl – 1.0 g; $MgSO_4 \cdot 5H_2O$ – 0.5 g at a temperature of 15–25 °C for 3-5 days under liquid-phase fermentation.

Yeast biomass – on Czapek's medium: per 1000 ml of water – sucrose 20 g, $NaNO_3$ –3.0 g; KH_2PO_4 – 1.0 g; KCl - 0.5 g; $MgSO_4 \cdot 7H_2O$ – 0.5 g at a temperature of 15-25 °C for 3-5 days under liquid-phase fermentation.

Microalgae biomass –on Tamiya medium: per 1000 ml of water – KNO_3-5.0; $FeSO_4 \cdot 7H_2O$ – 0.003 g; $MgSO_4 \cdot 5H_2O$ – 2.5 g; KH_2PO_4 – 1.25 gat a temperature of 15-25 °C for 3-5 days under liquid phase fermentation. The resulting suspensions were combined into a biological product "Biotrin".

Biogeosorbents were produced by processing analcime-bearing rocks with a particle size of 0.1–0.25 mm using *Biotrin* biological product (10^9 cell titer) in the ratio 1 part of the biological product to 6 parts of the sorbent.

Preparation of oil-contaminated water (control). 0.5 g of oil was added to 100 ml of Czapek's medium without sucrose. It was aerated in a shaker at 180 rpm for 4 days at room temperature and natural light. The water was filtered. The standards for maximum permissible concentration (MPC) of oil products in the waters of fishery water bodies are 0.05 mg/dm³ [29]. The oil content in the control water sample is 2.4 times higher than MPC.

Experiment conditions. Prepared oil-contaminated water was poured into 250 ml flasks and 1 g of the initial sorbents (without Biotrin) and biogeosorbents were added. The experiment was carried out for 4 days at room temperature, natural light, aeration on a shaker (180 rpm). The oil content in model water samples, filtered initial sorbents and biogeosorbents was analyzed by fluorimetry by Fluorat-02 fluid analyzer.

2.6 Modeling of biogeosorbents for phenol destruction

As phenol destructors, we used microalgae *Chlorella vulgaris* Beijer f. *globosa* V. Andr [28]. The microalgae strain was grown on Tamiya medium in Biostat® A MO UniVessel® Glass BB-8822000 2L 230V fermenter for 3-5 days under conditions of liquid-phase fermentation at 350 rpm, temperature 25–27 °C, pH 5.5–6.5, lighting byphytolamp175–250V 50 Hz until the titer of cells in a suspension of 108 cells/cm³ was reached. Tamiya medium (per 1 dm³ of deionized water) of the following composition: KNO_3 – 5 г, $KH_2PO_4 \times 3H_2O$ – 1.25 г, $MgSO_4 \times 7H_2O$ – 2.5 g, trace elements – 1 cm³ each. The trace element solutions are as follows (per 1 dm³ of deionized water).

1. Alkaline solution EDTA: EDTA – 50 g; KOH – 31 g.
2. Acidic iron solution: $FeSO_4 \times 7H_2O$ – 4.98 г, H_2SO_4 – 1cm³.
3. Boric acid solution: H_3BO_3 – 11.42 g.
4. The solution of trace elements: $ZnSO_4 \times 7H_2O$ – 8.82 г; $MnCl_2 \times 4H_2O$ – 1.44 г; MoO_3 – 0.71 г; $CuSO_4 \times 5H_2O$ – 1.57 г; $Co(NO_3)_2 \times 6H_2O$ – 0.49 g.

Then, a suspension microalgae was sprayed onto a mineral carrier (analcime-bearing rock) and dried at a temperature of 25 °C. The ratio of the composition of the biogeosorbent: mineral carrier is 85–90 %, the microalgae strain *C. vulgaris*– 10–15 %.

Microalgae cells were counted by Goryaev-Tom camera [30] under Biomed 3 microscope, binocular: BF, quadruple nose piece, Achromat 4x/10x/40x/100xMI lenses. The

dehydrogenase activity of the aqueous suspension was investigated in accordance with the methodology of the All-Russian Research Institute of Water Resources. The amount of phenols was analyzed by capillary gas chromatography [31].

3. Results and discussion

3.1 Mineralogical-petrographic studies

The analcime-bearing rocks are represented by Permian aleurolites, argillites and, more rarely, marls with many cavities filled by analcime partially or completely. Mineralogical and petrographic studies determined that oligomictic and polymictic *siltstones* were characterized by irregular spotted and irregular layered textures, due to the presence of layers and nests composed of material of both psammitic and pelitic dimensions. Clastic material, almost non-rounded and poorly sorted, is represented by quartz, feldspars, muscovite, fragments of effusive rocks. Authigenic minerals include, sericite, chlorite, and pyrite. Clay-micaceous and clay-carbonate cement are unevenly ferruginized.
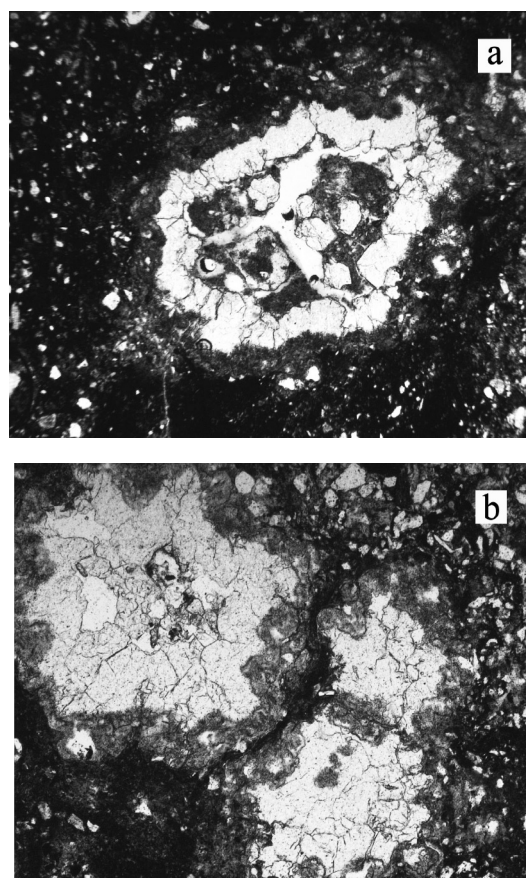
1. ábra   analcime által bemetszett üreg (a); komplex analcime aggregátumok, amelyek kitöltik az üregeket (b). Átlátszó vékony szakaszok. Magn. x200.
Fig. 1   The cavity incrusted by analcime (a); complex analcime aggregates filling cavities (b). Transparent thin sections. Parallel nicols. Magn. x200.

The argillites are also characterized by spotted and layered textures, caused, on the one hand, by uneven ferrugination, and, on the other, by the presence of rock layers consisting of psammite and silt grain. The microstructure of the clay material is scaly and felted. Fragments of quartz, feldspars, carbonates, effusive rocks, flakes of muscovite, chlorite, as well as pyrite and iron hydroxides are noted in the argillites.

Sample No.	Qtz	Ilt	Chl	Mlm	An	Clc	Fsp	Other phases
551	+	+	+	+	+	–	+	goethite
56403	+	+*	+	+	+	–	+	goethite
1/83	+	+	+	+	+	+	+	dolomite, kaolinite
58603	+	+*	+?	+	+	–	+	–

Note: Qtz – quartz, Ilt – illite, Chl – chlorite, Mlm – mixed-layer phase, Glt – glauconite, An – analcime, Clp – clinoptilolite, Clc – calcite, Fsp – feldspar; * - modified, hydrated mineral; ? - mineral is unreliable or minor.

1. táblázat   *Az analcimet hordozó kőzetek ásványi összetétele röntgendiffrakciós analízissel*
Table 1.   *Mineral composition of analcime-bearing rocks according to X-ray diffraction analysis*

Component	551	56403	1/83	58603
SiO_2	54.46	60.90	35.48	63.40
TiO_2	0.92	1.13	0.56	0.91
Al_2O_3	17.68	15.73	11.13	14.47
$Fe_2O_{3\ total}$	8.42	6.52	7.48	5.81
MnO	0.049	0.024	0.53	0.025
CaO	0.79	0.79	14.39	2.14
MgO	1.59	1.69	4.79	1.04
K_2O	2.16	2.20	1.69	1.43
Na_2O	4.34	3.49	1.83	3.28
P_2O_5	0.13	0.079	0.073	1.09
LOI	8.92	7.13	21.94	6.01
Total	99.46	99.68	99.89	99.61
FeO	0.31	0.62	1.23	<0.25
H_2O^-	2.42	1.67	2.52	1.34
CO_2	0.13	<0.1	15.34	0.42

2. táblázat   *Az analcimot hordozó kőzetek kémiai összetétele, wt. %*
Table 2   *Chemical composition of analcime-bearing rocks, wt. %*

Sample	Specific surface area, m²/g	C_{BET}	Total pore volume, cm³/g	Mesopore volume, cm³/g	Micropore volume, cm³/g	Average pore radius, nm
551	39.77	250.75	0.0436	0.0317	0.017	2.19
56403	25.00	298.96	0.0250	0.0169	0.010	2.00
1/83	38.59	287.09	0.0347	0.0218	0.016	1.79
58603	23.29	370.66	0.0205	0.0127	0.010	1.76

3. táblázat   *Az analcimet hordozó kőzetek fajlagos felülete és porozitása*
Table 3   *Specific surface area and porosity of analcime-bearing rocks*

Analcime, the content of which varies from 1 to 30 %, is present in the form of various-grained (from fine to coarse-grained) aggregates composed of well-faceted crystals. Analcime aggregates encrust round and oval cavities, and also fill microfractures in the rocks (*Fig. 1*). Different stages of filling voids are clearly traced – from insignificant incrustation to complete substitution.

According to X-ray diffraction analysis, layered silicates are diagnosed by weak reflexes and are probably represented by mixed-layer weakly ordered illite/smectite.

The mineral and chemical compositions of samples of analcime-bearing rocks are presented in *Tables 1* and *2*.

3.2 Sorption parameters

Textural characteristics are presented in *Table 3*. The specific surface of the samples is in the range 23.29–39.77 m²/g.

According to IUPAC classification [32], the nitrogen adsorption-desorption isotherms of analcime-bearing rocks are related to type IV (a) (*Fig. 2a*). They are characterized by the presence of a hysteresis loop and are typical of mesoporous sorbents. A sharp rise is observed in the adsorption curve at low pressures, indicating the presence of micropores in the sample (<2 nm). A rise in the adsorption curve at a relative pressure close to 1 indicates the presence of macropores. The hysteresis loop can be classified as types H3 and H4, since clay minerals and zeolites are also present in the sample. The pore size distribution curve is characterized by a narrow pore radius distribution in the range 0.8–4.0 nm with maxima 2.43–2.47 and 1.38–1.54 nm (*Fig. 2b*).

Promising areas for the use of analcime-bearing rocks are technologies for purification of water resources (drinking, domestic, storm, wastewaters) from heavy metals, organic substances, petroleum products, radionuclides.
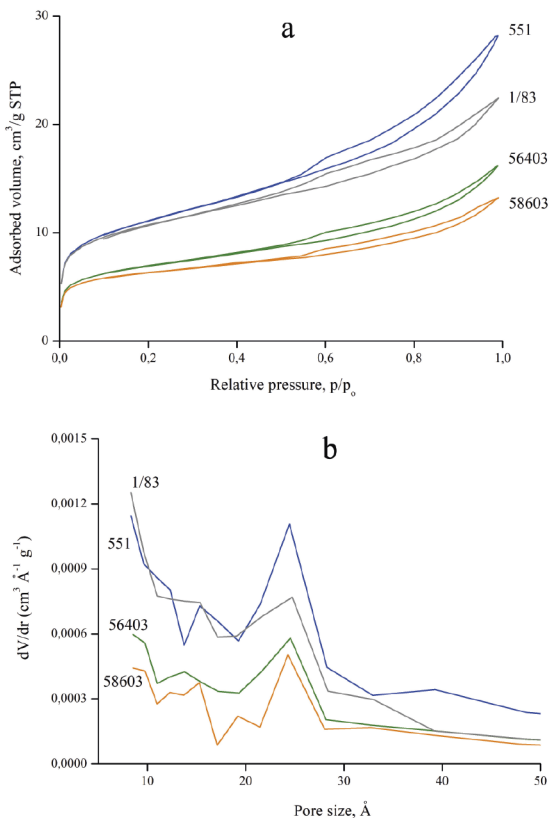
2. ábra Az analcimet hordozó kőzetek nitrogén-szorpciós-deszorpciós izotermái (a) és pórusméret-eloszlási görbéi (b)

Fig. 2 Nitrogen sorption-desorption isotherms (a) and pore size distribution curves (b) of analcime-bearing rocks

3.3 Sorption of natural radionuclides

The results of the study of sorption by analcime-bearing rocks are presented in *Table 4*. The data obtained show that analcime-bearing rocks completely absorb thorium from the solution. We revealed a high degree of extraction of radium (99.2–99.6 %) and uranium (98.8–99.4 %).

Fig. 3 shows the dynamics of sorption of uranium and radium by analcime-bearing rocks. Uranium sorption proceeds more vigorously, within 30 minutes more than 95 % of uranium is sorbed. More than 97 % of thorium is sorbed within 2.5 hours.

For natural radionuclides, present in natural solutions in ultramicroconcentrations and therefore unable to saturate the sorbent to the limit, an important characteristic is the absorption strength (or desorption) of elements or the compounds formed by them [24, 33].

As mentioned above, desorption was evaluated by the content of radionuclides in the extracts obtained by sequential treatment of the sorbent enriched with radionuclides with distilled water, 1M solutions of ammonium acetate and hydrochloric acid. When treated with distilled water, water-soluble salts, organic and inorganic compounds pass into the liquid phase. Exposure to ammonium acetate shows the tendency of absorbed radionuclides and their compounds to ion exchange. Stronger forms of radionuclides associated with mobile and stable oxides and soluble organic compounds are extracted with hydrochloric acid. It should be noted that in an acidic environment the destruction of the structure of zeolites

and clay minerals is possible, which results in the extraction of radionuclides in solution.
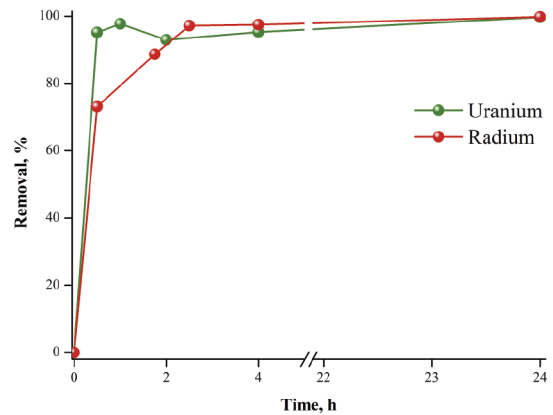
3. ábra Az urán és a rádium extrakciójának dinamikája analcimot hordozó kőzetekkel az oldatból

Fig. 3 Dynamics of the extraction of uranium and radium from the solution with analcime-bearing rocks

The results of the experiments showed (*Table 4*) that thorium was most firmly retained by the analcime-bearing rocks. We observed a small extraction into the solution upon interaction with water and ammonium acetate. So, when treated with distilled water, 2.0–2.7 % of thorium passes into the solution; when treated with ammonium acetate, 0–0.7 %. And only in an acidic environment we observed a significant desorption of thorium – from 47.4 to 60.0 %.

As a result of the action of ammonium acetate from the considered radioactive elements, radium is most prone to ion exchange, which results in its significant extraction into the solution from analcime-bearing rocks (47.0–53.2 %). When treated with water, radium is firmly retained by the analcime-bearing rocks – less than 0.3 % is desorbed. Acid treatment also supports recovery of radium.

Analcime-bearing rocks firmly retain uranium when treated with water: only 0.1–0.3 % of the radionuclide is recovered, but when exposed to ammonium acetate and acid, 18.1–21.0 and 29.5–34.0 % respectively pass into the solution, respectively.

The combination of high sorption ability with the ability to hold contaminants strongly is an important characteristic of the sorption material from the point of view of its practical use, since it allows avoiding secondary (reverse) contamination of the working environment with radionuclides. Fundamentally, sorbents can be used to trap and retain radionuclides in solutions over a wide range of radionuclide concentrations. It also increases the scope of sorption material – from low concentrated natural waters to highly radioactive liquid waste from nuclear power plants. The data obtained show the advisability of using these sorbents to solve environmental problems, including those associated with the rehabilitation of radiation-contaminated territories.

3.4 Sorption of pollutants in the treatment of drinking water and wastewater enterprises

Fig. 4 a-d presents results of drinking water purification from the Vychegda river during filtration through analcime-bearing rock and silica sand, which is currently used at a local

Sample	Removal, %	Desorption, %		
		Distilled water	**1M CH₃COONH₄**	**1M HCl**
		$1M\ CH_3COONH_4$		
Radium (initial concentration in solution $0.32 \cdot 10^{-10}$g/ml)				
551	99.6	0.01	52.33	30.93
56403	99.6	0.35	52.91	27.05
1/83	99.5	0.24	47.03	29.39
58603	99.2	0.91	53.24	25.04
Uranium (initial concentration in solution $0.8 \cdot 10^{-6}$g/ml)				
551	99.2	0.3	17.65	34.03
56403	99.4	0.17	20.96	33.54
1/83	98.8	0.21	18.99	29.54
58603	98.9	0.10	18.11	30.74
Thorium (initial concentration in solution $0.5 \cdot 10^{-6}$g/ml)				
551	100	2.33	0.00	51.33
56403	100	2.67	0.33	60.00
1/83	100	2.00	0.67	53.33
58603	100	2.67	0.33	47.33

4. táblázat   A természetes radionuklidok szorpciója analcimet hordozó kőzetek segítségével
Table 4   Sorption of natural radionuclides by analcime-bearing rocks
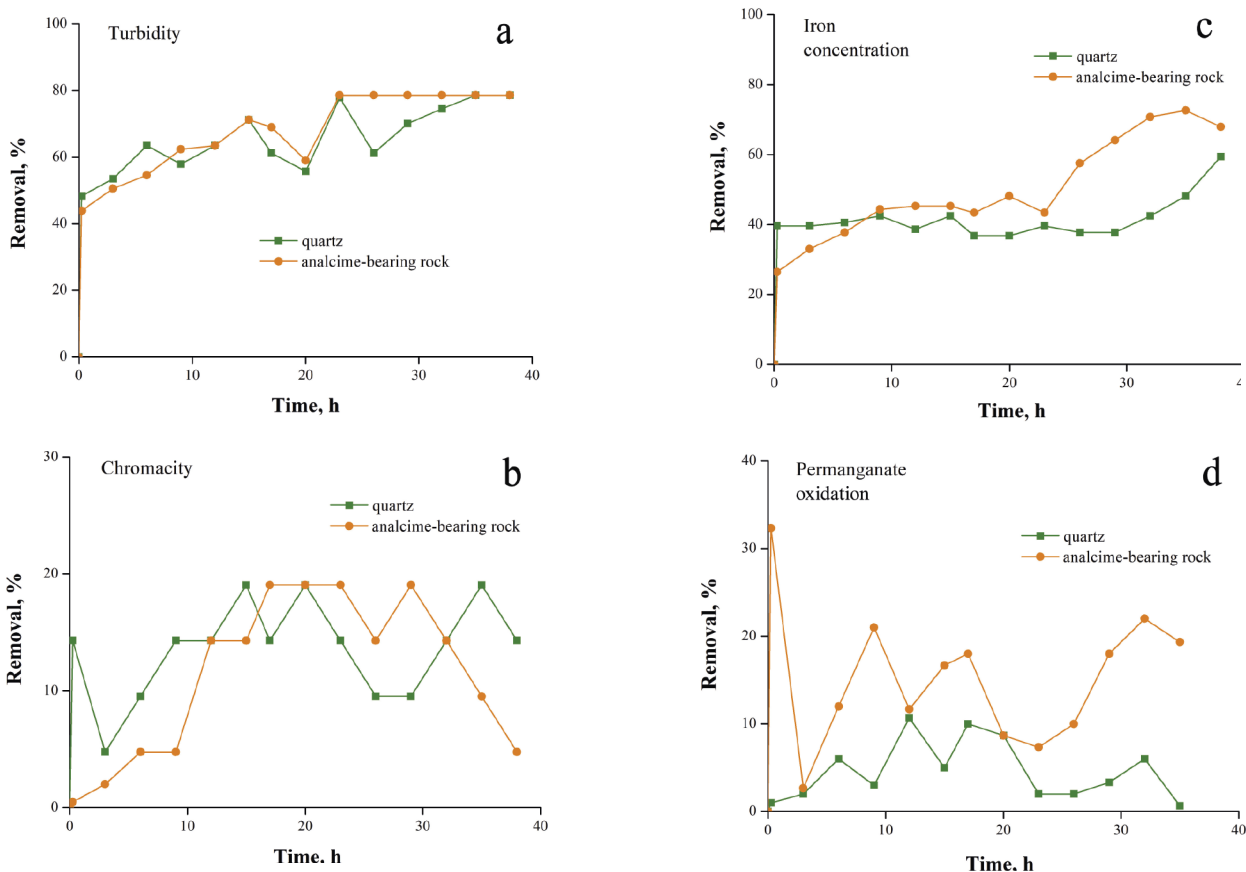
4. ábra   Zavarosság (a), krómképesség (b), vastartalom (c) és permanganát-oxidálhatóság (d), amikor a vizet szűrjük analcimet hordozó kőzet és kvarc homokon
Fig. 4   Turbidity (a), chromacity (b), iron content (c) and permanganate oxidability (d) when filtering water through analcime-bearing rock and quartz sand

water treatment plant. Both types of filter media approximately equally improve the organoleptic indicators of water quality: chromacity and turbidity decrease by 20 and 78 %, respectively. However, the analcime-bearing rock significantly reduces the iron content in water and permanganate oxidation: by 32 and 11 %, respectively [34, 35].

Table 5 presents results of wastewater treatment from boot factory (Vylgort town). The experiments revealed a significant decrease in the following indicators: suspended solids, turbidity, COD, ammonium, petroleum products, phosphates. Increasing pH of water from acidic (4.57) to neutral (7.32) was noted [7].

	pH	Suspended solids, mg/dm³	Turbidity	COD, mg/dm³	N-NH₄, mg/dm³	PO₄³⁻, mg/dm³	Oil products, mg/dm³	Anionic surfactants, mg/dm³
Before treatment	4.57	340	247	210	5.0	1.3	0.31	0.07
After treatment	7.32	100	3.2	61	0.25	0.46	0.049	0.06

5. táblázat   *A szennyvíz mutatói az analcimot hordozó kőzettel történő kezelés előtt és után*
Table 5   *Indicators of wastewater before and after treatment by analcime-bearing rock*

Initial samples	Content of oil products*	Biogeosorbents	Content of oil products*
551	0.04±0.014 / 250±60	**551-B**	0.11±0.04 / 57±23
56403	0.046±0.016 / 130±50	**56403-B**	0.061±0.021 / 37±15
1/83	0.048±0.017 / 250±60	**1/83-B**	0.071±0.025 / 220±90
58603	0.071±0.025 / 250±60	**58603-B**	0.064±0.022 / 90±40
Oil-contaminated water (control)	0.12±0.041		

Note: in the numerator, the content of oil products in the experimental water, mg/dm³, in the denominator – the content of oil products in the initial sorbents and biogeosorbents after the experiment, mg/g

6. táblázat   *Az olajtermékek vízben való koncentrációjának változása kezdeti analcimet hordozó kőzetek és biogeoszorbensek jelenlétében*
Table 6   *Change of concentration of oil products in water in the presence of initial analcime-bearing rocks and biogeosorbents*

Sample	Specific surface area, m²/g	
	Without degassing	With degassing at 25 °C, 2 hours
551	13.79	16.67
551B	13.65	8.24
56403	7.05	13.30
56403B	3.20	4.74
1/83	10.07	9.34
1/83B	10.98	8.88
58603	10.40	12.85
58603B	6.37	7.15

7. táblázat   *A kezdeti analimet tartalmazó hordozó kőzetek és biogeoszorbensek fajlagos felülete (szemcseméret 0,1–0,25 mm)*
Table 7   *Specific surface area of initial analcime-bearing rocks and biogeosorbents (grain size 0.1-0.25 mm)*

Lanina et al. [36] showed exploitability of using analcime-bearing rocks in the technological scheme of treatment of wastewaters from boilers of gas production department (Vuktyl town) as a granular filter load for removing mechanical impurities, organic compounds, nitrates, ammonium nitrogen, Fe ions with subsequent membrane cleaning. Lanina et al. [37, 38] revealed high absorptive characteristics of these rocks during the treatment of drilling wastewater generated during oil production.

3.5 Sorption and destruction of oil products by biogeosorents

For the northeast of the European part of Russia as an oil-producing region, the problems of contamination of territories with oil and oil products during exploration, production, transportation, storage and processing are very relevant. One of the ways to solve the problem is to use biogeosorbents based on zeolite-containing rocks as a carrier for microorganisms-oil destructors.

Table 6 presents results of a change in the concentration of petroleum products in model water in the presence of initial analcime-bearing rocks and biogeosorbents. Samples of the original analcime-bearing rock (551, 56403, 1/83) show adsorption activity against petroleum products. As a result of the introduction of these samples into oil-contaminated water,

the pollutant content in water decreases 2.5-3 times over 4 days, below the maximum permissible concentration.

When biogeosorbents (551-B, 56403-B, 1/83-B, 58603-B) are introduced into contaminated water, the efficiency of water purification decreases and does not reach MPC standards, which indicates decreasing sorption properties after immobilization of microorganism cells on mineral carriers. The decrease of the sorption properties of biogeosorbents is probably caused by a decrease in the specific surface area resulted from the adhesionally fixed biomass of microorganisms. This is confirmed by the experimental data on the determination of the specific surface area of the initial analcime-bearing rocks and biogeosorbents (*Table 7*). In almost all cases, the specific surface area of the initial sorbents is higher than the specific surface of biogeosorbents. When microorganisms are immobilized on analcime-bearing rocks, the specific surface area decreases 1.1–2.8 times.

The analysis of the water part of microcosms after introducing samples of both the original analcime-bearing rocks and biogeosorbents based on them showed that, with significantly high water purification, the differences between the sorbent/biogeosorbent variants are insignificant, and significant differences were noted in sample 551. Biodegradation of oil products by biogeosorbents for 4 days ranged from 12 to 77 % [39, 40].

3.6 Sorption and destruction of phenols by biogeosorbents

We evaluated sorption and destructive properties of initial sorbents, a suspension of microalgae *Chlorella vulgaris*, and simulated biogeosorbents in relation to phenols (initial concentration 10 µg/dm³) (*Table 8*). We revealed the advantage of the synergetic complex of the biogeosorbent from its individual components: a decrease in the period of water purification from phenols. Biodegradation of 83 % of phenols in model water occurs in 3 days.

	3 days	45 days
C0	8.34	–
EC	7.42	3.0
MA	2.16	0.83
A	1.85	0.21
AMA	1.07	0.19

Note: C0 – zero control, EC – experimental control, MA – microalgae, A – analcime-bearing rocks, AMA – analcime-bearing rock with immobilized microalgae

8. táblázat   A fenolkoncentráció vízben (µg/dm3) mikroalgákkal, analcimet hordozó kőzettel és biogeoszorbenssel való kölcsönhatás után

Table 8   Phenol concentration in water (µg/dm³) after interaction with microalgae, analcime-bearing rock and biogeosorbent

The biogeosorbent was tested for resistance to stress factors: relatively high temperatures, conditions of high salinity and the influence of organic pollutants. For this, samples of the biogeosorbent were thermostated at a temperature of 80 °C, introduced into model phenolic water (concentration 10 µg/dm³) and sea water (salinity 34 ‰).

The mineral carrier provides safety and increases growth of microalgae cells under stressful conditions. Microalgae *Chlorella vulgaris*, immobilized on analcime-bearing rock, show tolerance to increased salinity and organic pollutants. However, during thermostating of the biogeosorbent, no living microalgae cells were found [41].

4. Conclusions

The results obtained show the potential of using analcime-bearing rocks in the north-east of the European part of Russia in sorption processes.

We determined a high sorption activity with respect to radioactive elements: degree of absorption of radium, uranium, and thorium was up to 99.6, 99.4, and 100%, respectively. The study of desorption characteristics showed that sorbents had a sufficiently high absorption strength (or low total desorption).

We showed prospects of using these rocks in the treatment of drinking and wastewater of enterprises. It is possible to use them in a sorption-filtering material for purification of household waters in quick filters of water intake structures instead of quartz sand.

We evaluated sorption and destructive properties of initial analcime-bearing rocks and modeled biogeosorbents in relation to oil products. We determined that samples of initial sorbents showed a high adsorption activity in relation to oil products, reducing oil content by 2.5–3 times (to norms or significantly lower than MPC norms).

When immobilizing microorganism cells on the surface of analcime-bearing rocks, a decrease in sorption properties was revealed, but at the same time, microorganisms provided biodegradation of hydrocarbons, which amounted to 77 % in 4 days.

Analcime-bearing rocks provide safety and increases growth of microalgae cells under stressful conditions. Microalgae *Chlorella vulgaris*, immobilized on analcime-bearing rocks, show tolerance to increased salinity (salinity 34 ‰) and phenols (concentration 10 µg/dm³).

The advantage of the synergetic complex of the biogeosorbent in comparison to individual components is revealed: a decrease in the period of water purification from phenols. Biodegradation of 83 % of phenols in model water occurs in 3 days.

Acknowledgments

References

[1] Tazić, Z. Z. – Bogdanović, G. D. – Antonijević M. M. (2019): Application of natural zeolites in wastewater treatment – A review. Journal of Mining and Metallurgy A: Mining. Vol. 55, 1, pp. 67–79.

[2] Williams, C. D. (2018): Applications of zeolites to environmental remediation. Chapter in book Urban pollution: Science and Management. First Edition. Edited by Susanne M. Charlesworth and Colin A. Booth. pp. 249–258.

[3] Yona, Z. (2016): Review of the natural, modified and synthetic zeolites for heavy metal removal from wastewater. Environmental Engineering Science. Vol. 33, No. 7. pp. 443–454. https://doi.org/10.1089/ees.2015.0166

[4] Misaelidis, P. (2019): Clay minerals and zeolites for radioactive waste immobilization and containment: a concise overview. Chapter in book Modified Clays and Zeolites nanocomposite materials. pp. 243–274. https://doi.org/10.1016/B978-0-12-814617-0.0004-9

[5] Demirkiran, A. R. – Fullen, M. – Williams, C. (2016): Physicochemical and oil adsorption characteristics of zeolites: clinoptilolites (review). Oxidation Communications. 39, No. 3-II, pp. 2704–2721.

[6] Kalita, B. – Bora, S. S. – Gogoi, B. (2020): Zeolite: a soil conditioner. International Journal of Current Microbiology and Applied Sciences. Vol. 9, No. 1, pp. 1184–1206. https://doi.org/10.20546/ijcmac.2020.901.133

[7] Kotova, O. B. – Harja, M. – Cretescu, I. – Noli, F. – Pelovski, Y. – Shushkov, D. A. (2017): Zeolites in technologies of pollution prevention and remediation of aquatic systems. Vestnik of the Institute of Geology, Komi SC, UB RAS. No. 5. pp. 49–53. https://doi.org/10.19110/2221-1381-2017-5-49-53

[8] Dalang, S. – Mohd Tuah, P (2016): Removal of phenol byzeolite. Transactions on Science and Technology. Vol. 3(1-2), pp. 107–113.

[9] Chaouati, N. – Soualah, A. – Chater, M. (2013): Adsorption of phenol from aqueous solution onto zeolite Y modified by silylation. Comptes Rendus Chimie. Vol. 16, Iss. 3, pp. 222–228. https://doi.org/10.1016/j.crci.2012.10.010

[10] Coombs, D. S. – Albert, A. – Armbruster, T – et al (1997): Recommended nomenclature for zeolite minerals: report of the Subcommittee on Zeolites of the IMA, Commission on New Minerals and Mineral Names. The Canadian Mineralogist. Vol. 35, pp. 1571–1606.

[11] Colella, C. – Wise, W. S. (2014): The IZA Handbook of Natural Zeolites: A tool of knowledge on the most important family of porous minerals. Microporous and Mesoporous Materials. Vol. 189, pp. 4–10.

[12] Margeta, K. – Logar, N. Z. – Šiljeg, M. – Farkaš, A. (2013): Natural zeolites in water treatment – how effective is their use. Chapter in book Water Treatment. Pp. 81–112. https://doi.org/10.5772/50738

[13] Chica, A. (2013): Zeolites: promised material for the sustainable production of hydrogen. ISRN Chemical Engineering. Article ID 907425. 19 p. https://doi.org/10.1155/2013/907425

[14] Yusupov, T. S. – Shumskaya, L. G. (2009): A new concept for the production of aluminum and its compounds from non-traditional aluminosilicate raw materials. Phizico-tekhnicheskie Problemy Razrabotki Poleznyh Iskopaemyh (Physicotechnical Problems of Mining). No. 2, pp. 96–100. (In Russian)

[15] Razmakhnin, K. K. – Khatkova, A. N. (2014): Modern technologies of processing and modification of zeolite-bearing rocks of East Transbaikalia. Chita: ZabSU. 310 p. (In Russian)

[16] Khatkova, A. N. – Razmakhnin, K. K. – Emelyanov, V. N. (2013): The possibility of extracting aluminum from zeolite-bearing rocks of East Transbaikalia. Vestnik of IrGTU No. 2, pp. 95–100. (In Russian)

[17] Silaghi, M.-C. – Chizallet, C. – Sauer, J. – Raybaud, P. (2016): Dealumination mechanisms of zeolites and extra-framework aluminum confinement. Journal of Catalysis. 339, pp. 242–255. http://dx.doi.org/10.1016/j.jcat.2016.04.021

[18] Shushkov, D. A. – Kotova, O. B. – Goldin, B. A. (2011): Geomaterials on the basis of analcime-bearing rocks. Geomaterials. No. 1, pp. 33–40. http://dx.doi.org/10.4236/gm.2011

[19] Razmyslov, I. N. – Kotova, O.B. – Silaev, V. I. – Rostovtsev, V. I. – Kiseleva, D. V. –Kondratiev, S. A. (2019): Microphase heterogenization of glandular bauxite as a result of radiation-thermal treatment. FTPRPI. No. 5, pp. 128–140. (In Russian) http://dx.doi.org/10.15372/FTPRPI20190514

[20] Shchipalkina, N. V. – Pekov, I. V. – Koshlyakova, N. N. – Britvin, S. N. – Zubkova, N. V. – Varlamov, D. A. – Sidirov, E. G. (2020): Unusual silicate mineralization from fumarolic sublimates of the Tolbachik volcano, Kamchatka, Russia. Part I. Ino-, cyclo-, neso-, phyllosilicates. European Journal of Mineralogy. Vol. 32, pp. 101–119.

[21] Shchipalkina, N. V. – Pekov, I. V. – Koshlyakova, N. N. – Britvin, S. N. – Zubkova, N. V. – Varlamov, D. A. – Sidirov, E. G. (2020): Unusual silicate mineralization from fumarolic sublimates of the Tolbachik volcano, Kamchatka, Russia. Part II. Tectosilicates. European Journal of Mineralogy. Vol. 32, pp. 121–136.

[22] Sitnikov, P. A. – Kuchin, A. V. – Belykh, A. G. – Vaseneva, I. N. – Ryabkov, Yu. I. (2011): Preparation of epoxy composite material containing natural aluminosilicate filler. Polymer Science, Series D. Glues and Sealing Materials. Vol. 4, No. 4, pp. 281–283. https://doi.org/10.1134/S1995421211040125

[23] Kotova, O. B. – Shushkov, D. A. – Gömze, L. A. – Kurovics, E. – Ignatiev, G. V. – Sitnikov, P. A. – Ryabkov, Yu. I. – Vaseneva, I. N. (2019): Composite materials based on zeolite-montmorillonite rocks and aluminoslicate wastes. Építöanyag – Journal of Silicate Based and Composite Materials. Vol. 71, No 4, pp. 125–130. https://doi.org/10.14382/epitoaniag-jsbcm.2019.22

[24] Rachkova, N. G. – Shuktomova, I. I. (2006): The role of sorbents in the processes of transformation of uranium, radium, and thorium compounds in podzolic soil. St. Petersburg: Nauka.146 p.

[25] Conclusion about toxicological and hygienic assessment of Biotrin consortium of oil-oxidizing microorganisms strains. SIC TBP branch «State Research Center Institute of Immunology» Serpukhov, 09/28/2017. (In Russian)

[26] RU Patent 2615458. The bacterial strain Pseudomonas yamanorum VKM B-3033D for activating the biodegradation of petroleum and petroleum products in water, as well as in oil soils in railway sections / BIOECOBALANCE LLC; Meshkelo, S.M. – Schemelinina, T. N. – Anchugova, E. M. – Markarova, M. Yu. – Zheludkova, S. V. Stated 10/08/2016; Publ. 04/04/2017, Bull. No. 10. (In Russian)

[27] RU Patent 2658134. The strain of the yeast Rhodotorula glutinis for the purification of oil-contaminated soils, ponds and wastewater from petroleum hydrocarbons, including for the oxidation of polyaromatic compounds / BIOECOBALANCE LLC; Meshkelo, S. M. – Schemelinina, T. N. – Markarova, M. Yu. – Anchugova, E. M. Stated 07/02/2016; Publ. 06/20/2018, Bull. No. 17.

[28] RU Patent 2703499. Microalgae strain Chlorella vulgaris Beijer. f. Globosa V. Andr. For the purification of natural reservoirs and wastewater of industrial enterprises / Schemelinina, T. N. – Anchugova, E. M. – Gogonin, A. V. – Tarabukin, D. V. –Shapenkov, D. M.. Published: 10/17/2019, Bull. No. 29.

[29] On approval of water quality standards for water bodies of fishery importance, including standards for maximum permissible concentrations of harmful substances in the waters of water bodies of fishery value: Order of the Ministry of Agriculture of the Russian Federation of December 13, 2016. No. 552. URL: http://docs.chdt.ru

[30] Benjumovich, M. S. (2001): The application of Poisson units to the determination of median lethal cell culture dose. Toxicology in Vitro. Vol. 15, Iss. 6, pp. 671–675. https://doi.org/10.1016/S0887-2333(01)00086-8

[31] The method of measuring the mass concentration of phenol by capillary gas chromatography. No. 88-17641-006-2013 (FR.1.31.2013.15054). 2013 Edition (In Russian)

[32] Thommes, M. – Kaneko, K. – Neimark, A. V. – Olivier, J. P. – Rodriguez-Reinoso, F. – Rouquerol, J. – Sing, K. S. W. (2015): Physisorption of gases, with special reference to the evaluation of surface area and pore size distribution (IUPAC Technical Report). Pure and Applied Chemistry. Vol. 87, Iss. 9–10. pp. 1051–1069. https://doi.org/10.1515/pac-2014-1117

[33] Shushkov, D. – Kotova, O. – Shuktomova, I. (2013): Removal of radionuclides by analcime-bearing rocks. J. Material Science and Engineering. Vol. 47, pp. 198–202. http://doi.org/10.1088/1757-899X/47/1/012041

[34] RU Patent 2296718. The method of water purification / Shushkov, D. A. – Kotova, O. B. – Palshin, I. P. Stated July 7, 2005. Published. 04/10/2007. (In Russian)

[35] Shushkov, D. A. – Kotova, O. B. – Kapitanov, V. M. – Ignatiev, A. N. (2006): Analcime-bearing rocks of Timan as a promising type of minerals. Syktyvkar. 40 p. (Scientific recommendations - to the national economy / Komi Scientific Center, Ural Branch of the Russian Academy of Sciences; issue 123). (In Russian)

[36] Lanina, T. D. – Varfolomeev, B. G. (2007): The use of natural zeolite for post-treatment of wastewater from boiler houses of the Vuktylsky gas production department // Construction of oil and gas wells on land and at sea. No 8, pp. 38–40. (In Russian)

[37] Lanina, T. D. (2009): The use of natural sorbents for drilling wastewater treatment. Construction of oil and gas wells on land and at sea. No 9, pp. 55–56. (In Russian)

[38] Lanina, T. D. – Nosov, G. A. – Donin, S. N. (2017): The use of natural sorbents for wastewater treatment of industrial enterprises. Petroleum Engineer. No. 3, pp. 43–47. (In Russian)

[39] Schemelinina, T. N. – Kotova, O. B. – Harja, M. – Anchugova, E. M. – Pelovsky, I. – Cretescu I. (2017): New trends in the mechanisms for increasing the productivity of materials based on minerals. Vestnik of the Institute of Geology, Komi SC, UB RAS. No. 6, pp. 40-42. http://doi.org/10.19110/2221-1381-2017-6-40-42

[40] Shchemelinina, T. N. – Gömze, L. A. – Kotova, O. B. – Ibrahim, J. E. F. M. – Shushkov, D. A. – Harja, M. – Ignatiev, G. V. – Anchugova, E. M. (2019): Clay- and zeolite-based biogeosorbents: modeling and properties. Építöanyag – Journal of Silicate Based and Composite Materials. Vol. 71, No. 4, pp. 131–137. https://doi.org/10.14382/epitoanyag-jsbcm.2019.23

[41] Shchemelinina, T. N. – Anchugova, E. M. – Kotova, O. B. – Sun, S. – Shushkov, D. A. – Gogonin, A. V. – Likhanova, N. V. – Zueva, O. M. – Korchagina, Yu. S. (2020): Why mineral carriers are necessary for microalgae. Vestnik of Geosciences. No 2, pp. 24–28. http://doi.org/10.19110/geov.2020.2.4

Effect of temperature on the structural properties of barium titanate nanopowders synthesis via sol-gel process

MOHAMMED TIHTIH ▪ Institute of Ceramics and Polymer Engineering, University of Miskolc, Hungary ▪ medtihtih@gmail.com

ALEKSEI V. PONARYADOV ▪ Institute of Geology, Komi Science Center, Ural Branch of the Russian Academy of Sciences, Russian Federation ▪ avponaryadov@geo.komisc.ru

JAMAL ELDIN F. M. IBRAHIM ▪ Institute of Ceramics and Polymer Engineering, University of Miskolc, Hungary ▪ jamalfadoul@gmail.com

EMESE KUROVICS ▪ Institute of Ceramics and Polymer Engineering, University of Miskolc, Hungary ▪ fememese@uni-miskolc.hu

ELENA L. KOTOVA ▪ Saint-Petersburg Mining University, Russian Federation ▪ kotova_el@pers.spmi.ru

LÁSZLÓ A. GÖMZE ▪ Institute of Ceramics and Polymer Engineering, University of Miskolc, Hungary, IGREX Engineering Service Ltd ▪ femgomze@uni-miskolc.hu

Mohammed TIHTIH
Is graduated from Sidi Mohamed Ben abdellah University /Faculty of sciences Dhar El Mahraz, Fez, Morocco, Department of Physics, for the time being, he is a PhD student in the University of Miskolc, Institute of Ceramics and Polymer Engineering, under supervision of Prof. L. A. Gömze

Aleksei V. PONARYADOV
Is a Researcher of Laboratory of Technology of Mineral Raw, Institute of Geology, Komi Science Center, Ural Branch of the Russian Academy of Sciences. Author and co-author of more than 30 scientific articles. Russian Mineralogical Society

Jamal Eldin F. M. IBRAHIM
Is a lecturer in the University of Bahri, Khartoum, Sudan, he graduated from University of Marmara, Istanbul, Turkey, Institute of Pure and Applied Sciences, Department of Metallurgical and Materials Engineering, for the time being, he is a PhD student in the University of Miskolc, Institute of Ceramics and Polymer Engineering, under supervision of Prof. L. A. Gömze

Emese KUROVICS
Is graduated from the University of Miskolc, Department of Ceramics and Silicate Engineering as a material engineer, where she continues her study as PhD student under supervision of Prof. L. A. Gömze.

Elena L. KOTOVA
Is a Scientific Director of the Mining Museum of the Saint-Petersburg Mining University. Author and co-author of chapter in book, patent and more than 30 articles. The member of the Russian Mineralogical Society, Oil and Gas Historical Society of Russia

László A. GÖMZE
Is establisher and professor of the Department of Ceramics and Silicate Engineering in the University of Miskolc, Hungary. He is author or co-author of 2 patents, 6 books and more than 300 scientific papers.

Abstract

Sol-gel processed barium titanate ($BaTiO_3$) ceramic has been characterized by X-ray diffraction (XRD) and Fourier Transformation Infrared (FT-IR) techniques. The results confirm that $BaTiO_3$ crystallizes in the perovskite structure with Ba_2TiO_4 pyrochlore phase when calcined at relatively low temperature (800 °C) for 3h. Furthermore, XRD reveals the formation of a single-phase perovskite $BaTiO_3$ without presence of secondary phases when calcined at the temperature of 900 and 1000°C with the following lattice parameters: a = 3.9978Å, c = 4.0197Å and a = 3.9967Å, c = 4.0220Å respectively. the calcination temperature is confirmed to has a large influence in $BaTiO_3$ structure, several parameters including, the tetragonality, volume (V) and crystallite size were found to be increased with increasing calcination temperature.

Keywords: Sol-gel, Barium titanate nanoceramics, Calcination temperature, X-ray Diffraction.
Kulcsszavak: Szol-gél, bárium-titanát nanokeramika, kalcinációs hőmérséklet, röntgendiffrakció.

1. Introduction

The popularity of the research in the area of high-tech ceramics has attracted a great interest lately [1-22]. Barium titanate ($BaTiO_3$) is the most frequently utilized ferroelectric material, and even after seventy-five years of its disclosure, it remained as the most essential material which has excellent dielectric, optical, piezoelectric and ferroelectric properties [23]. Since the discovery of the phenomenon of ferroelectricity, $BaTiO_3$ has been a standard material in the family of ferroelectric perovskites. This compound has been used for a long time in many industrial sectors such as Multilayer Ceramic Capacitors (MLCCs) [24]. An interesting and very current application of $BaTiO_3$ concerns the creation of computer memories FRAMs (Ferroelectric Random Access Memories) [25]. The manufacture of thermistors and the detection of polluting gases such as CO also constitute applications of $BaTiO_3$. The properties, both optical and electrical, have proved to be very promising technologically, for example, the linear resonator, the sensors, the actuators, the phasing of laser sources, spatial light modulators, the guides of waves, holographic storage and high filters frequencies etc…) [26]. However, multilayer capacitors have long occupied the first place in $BaTiO_3$ applications.

Also, it is one of the most extensively studied lead-free ferroelectric materials due to its broad range of device applications including, capacitors, transducers, non-volatile memories, positive temperature coefficient (PTC) thermistors and many more. Due to the importance of $BaTiO_3$ which meet the requirements of miniaturization of integrated circuits in the field of electronics, new preparation techniques have been developed and successfully used to produce $BaTiO_3$ at lower temperatures compared to the solid path, which results in an appreciable gain in energy and enable the production of cost-effective metal or alloy electrodes. Among these techniques: it's worth mentioning the sol-gel method [27-29], the hydrothermal method [30] and the co-precipitation [31]. Through these methods a high purity $BaTiO_3$ with very fine and controllable particles size can be obtained. Furthermore, it is possible to easily modify the physical properties of BT since it is very sensitive to the doping on Ba site, Ti site and or a substitution (co-doping) coupled to the two sites, which enable their adaptations to very specific applications. In this work, BT materials were synthesized using sol-gel method and after it was calcined at temperatures of 800 °C, 900 °C, and 1000 °C. The aims of this research work are to determine the effects of calcining temperatures on Physical parameters such as lattice parameters, crystallite size and bands absorption of BT using X-ray diffraction (XRD) and Fourier Transformation Infrared (FT-IR).

2. Experimental procedure

In the present work, $BaTiO_3$ was prepared using sol-gel method. Barium acetate (Ba $(C_2H_3O_2)2•H_2O$, Aldrich, 99.9%) and titanium alkoxide ((Ti [OCH $(CH_3)_2]_4$, Aldrich, 97.9%) have been used as precursors, lactic acid (CH_3CH (OH) CO_2H, Aldrich, 90%) was used as peptizing agent, acetic acid was added to dissolve the barium acetate, and distilled water as a solvent. First, the titanium alkoxide was added to lactic acid aqueous solution and H_2O with continuous stirring at 70 °C. After 24 hours of reaction, the obtained white precipitate is transformed into clear homogeneous solution. In the second step the barium acetate was added to this colloidal solution in stoichiometric quantities. The obtained nanopowders were calcined in air for 3hrs at 800, 900 and 1000 °C with a heating rate of 5 °C/min. The different processing steps for the synthesis of $BaTiO_3$ nanopowders is shown in *Fig. 1*.
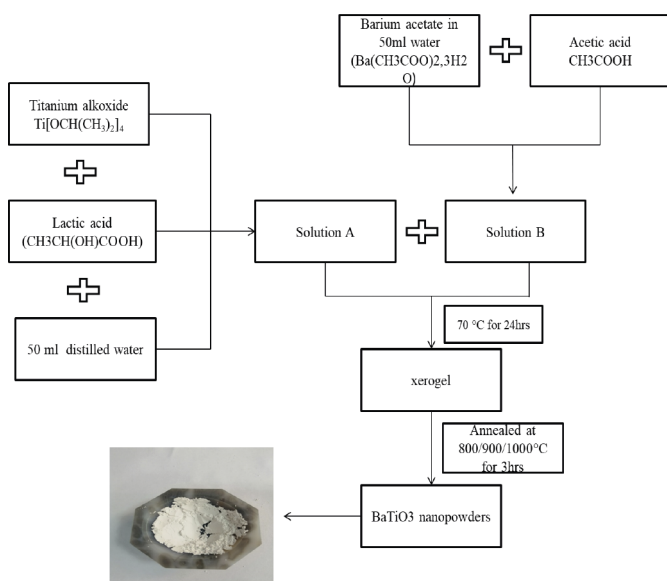

1. ábra   *A BaTiO3 nanoporok szintézisének folyamatábrája*
Fig. 1   *Flow chart of synthesis of $BaTiO_3$ nanopowders*

3. Results and discussion

3.1 X-ray Diffraction

The XRD analysis of the prepared samples was carried out at room temperature using (XPERT-PRO) diffractometer with CuKα (λ =1.5406 Å) radiation. The XRD patterns of the calcined pure BT powders recorded at 800 °C, 900 °C and 1000 °C are presented in *Fig. 2*. It is clearly observed that the XRD diffractogram of the powder prepared at 800°C is characterized by the appearance of the Ba_2TiO_4 pyrochlore phase [32]. Moreover, at temperatures of 900 °C and 1000 °C, the disappearance of the pyrochlore phase and the appearance of the pure perovskite phase are noticed. However, the analysis of the XRD spectra shows the juxtaposition of the two peaks (002) and (200) at the position 2θ = 44.93° for the temperature of 800 °C (*Fig. 3*). When the calcination temperature increases (T = 1000 °C) the two peaks separate. The presence of these two peaks shows a transition to the quadratic phase based on the temperature [33].
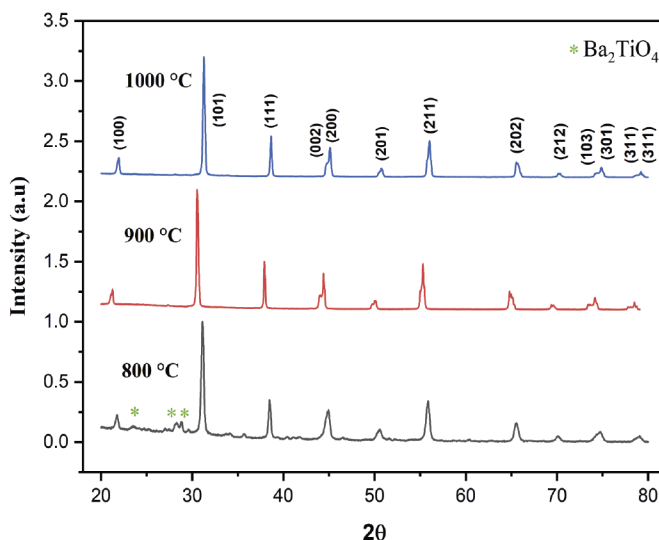
2. ábra   *A BaTiO3 nanorészecskék röntgendiffrakciós spektrumai különböző hőmérsékleteken: 800 °C, 900 °C és 1000 °C*
Fig. 2   *X-ray diffraction spectra of $BaTiO_3$ nanoparticles at different temperatures: 800°C, 900°C and 1000 °C*
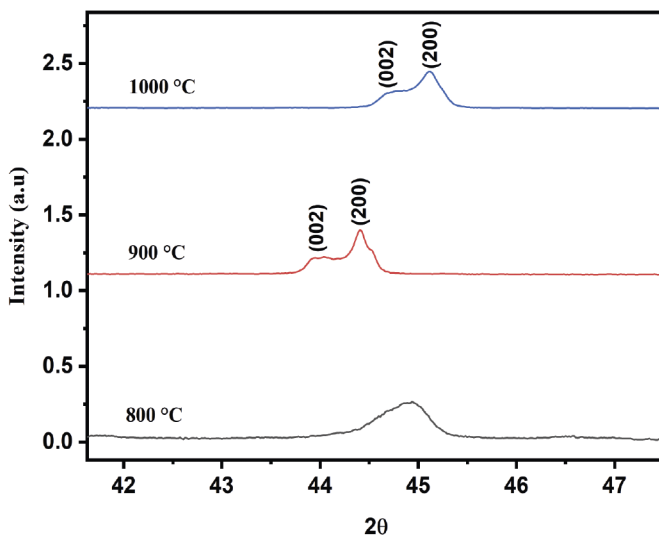
3. ábra   *A (002) és (200) csúcsok XRD mintája*
Fig. 3   *XRD patterns shifting of the peak (002) and (200)*

To better highlight the effect of the calcination temperature on the structural properties of BT, the lattice parameters, as well as the crystallite size for each calcination temperature were calculated. The prominent peaks were used to estimate the size of the nanoparticles through the Scherrer equation, expressed as follows [34]:

$$D = \frac{0.9\lambda}{\beta \cos \theta}$$

Where β is the full width at half maximum (FWHM) of the (101) peak, θ is the diffraction angle and λ is the X-ray wavelength (λ= 1.542 Å).
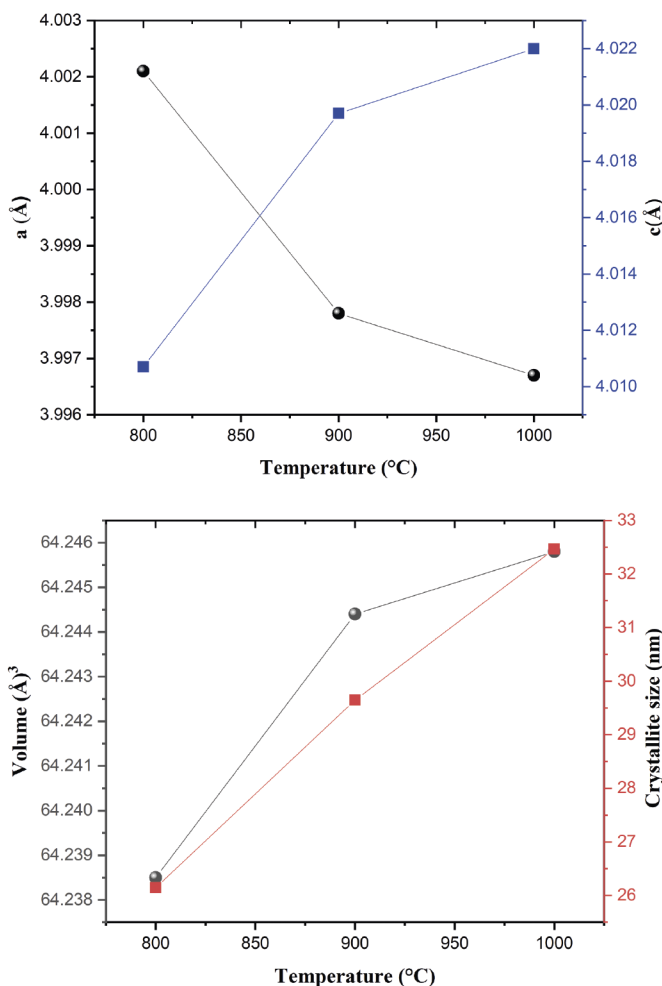
The evolution of the lattice parameters a and c, tetragonality, the volume (V) of the unit cell, and the crystallite size as a function of the calcination temperatures are listed in *Table 1* and represented in *Fig. 4*. This evolution is in agreement with those obtained by Teraoka et al [35] and Lombardo et al [36];

a higher calcination temperature results in the formation of larger crystallite size. In particular, the increase in particle size is relatively large for the sample calcined at 1000 °C. In *Table 1*, the estimated average size is 26.1455 nm and 32.4634 nm for the samples calcined at 800 and 1000 °C respectively. The characteristics of the crystallite size and the volume (V) of the unit cell have shown great similarity which indicates that the defects stimulated by the temperature can highly influence all the physical behaviours of $BaTiO_3$.

Annealed temperature (°C)	a=b (Å)	c (Å)	c/a	Volume (Å)³	Crystallite size (nm)	Phase / Space group
800	4.0021	4.0107	1.0021	64.2385	26.1455	-
900	3.9978	4.0197	1.0054	64.2444	29.6457	Tetragonal/ P4mm
1000	3.9967	4.0220	1.0063	64.2458	32.4634	Tetragonal/ P4mm

1. táblázat *Az BaTiO₃ egységcellák paraméterei, kristály mérete és szerkezete a hőmérséklettől függően*
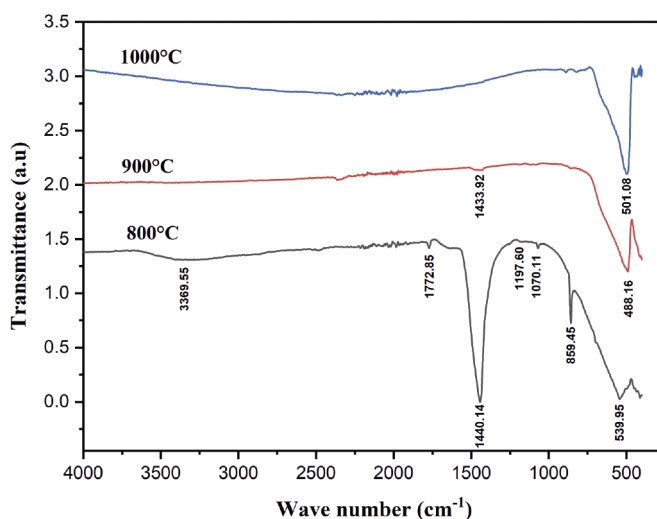
Table 1 *Unit cell parameters, Crystallite size and structure phase of BaTiO₃ versus temperature*

4. ábra *A BaTiO3 nanorészecskék rács paraméterei és kristály mérete a hőmérséklet függvényében*

Fig. 4 *Variation of the lattice parameters and the crystallites size of BaTiO₃ nanoparticles as a function of temperature*

3.2 FT-IR analysis

5. ábra *A BaTiO3 nanorészecskék FT-IR spektrumai különböző hőmérsékleteken: 800 °C, 900 °C és 1000 °C*

Fig. 5 *FT-IR spectrums of BaTiO₃ nanoparticles at different temperatures: 800°C, 900°C and 1000°C.*

Fig. 5 shows the infrared curves of barium titanate calcined at different temperatures. it can be noticed that these spectra present a set of absorption bands: a wide band of high-intensity located between 3700 and 2500 cm⁻¹ (3369 cm⁻¹) at 800 °C, as well as a fine peak located at 1772 cm⁻¹ of low-intensity indicating the presence of molecular water in the samples. The two more intense peaks located around 441 and 543 cm⁻¹ and the low-intensity peak correspond to the symmetrical stretching of the Ti-O bond [37], the characteristic of these peaks confirm the formation of pure tetragonal phase. These results are in agreement with the literature [38]. The intensity peak at 859 cm⁻¹ corresponds to a Ba-O elongation [39]. The two peaks located around 1440 and 1433 cm⁻¹ correspond to the symmetrical stretch of the C-O bond and the Ti-O-C bond respectively [37]. Note that the intensity of the peaks located at around 1772, 1644 and 859 cm⁻¹ decreases with increasing calcination temperature, this indicates that the barium titanate preparation was completed at 1000 °C.

4. Conclusions

Nanopowders of $BaTiO_3$ perovskite materials have been successfully prepared by using the sol-gel method at a temperature of 800 °C, 900 °C and 1000 °C. The prepared samples were characterized using XRD and FT-IR spectroscopy. The prepared samples were calcined at 900 °C, XRD analysis of the samples shows the presence of a single tetragonal phase without any secondary phase. At 1000 °C a slight distortion occurred, as showed on the determined unit cell parameters calculated from the corresponding XRD spectrum, which gave rise to the single tetragonal perovskite phase (space group P4mm). The observed change in the structural properties of $BaTiO_3$ was also examined via FT-IR spectrum and then confirmed by XRD analysis that show a gradual change in the recorded spectra in the temperature range of 800 °C to 1000 °C.

The disappearance of the absorption bands indicated the formation of BaTiO$_3$ structure and shows the effect of annealed temperature on the structural properties of BaTiO$_3$.

Acknowledgements

References

[1] Gömze, L. A.: 2016. Applied materials science I. Compilation of Selected Scientific Papers 1-189.

[2] Gömze, L. A. – Gömze, L. N.: 2013 IOP Conf. Ser.: Mater. Sci. Eng.47 012033. https://doi.org/10.1088/1757-899X/47/1/012033

[3] Gömze, László A. et al: 2019 IOP Conf. Ser.: Mater. Sci. Eng.613 012005. https://doi.org/10.1088/1757-899X/613/1/012005

[4] Kurovics, Emese et al: 2019 IOP Conf. Ser.: Mater. Sci. Eng.613 012025 https://doi.org/10.1088/1757-899X/613/1/012025

[5] Gömze, L. A. – Gömze, L. N.: 2008 Építőanyag–JSBCM **60** (4) 102 http://dx.doi.org/10.14382/epitoanyag-jsbcm.2008.16

[6] Hamza, A. et al: 2019 IOP Conf. Ser.: Mater. Sci. Eng. 613 012051 https://doi.org/10.1088/1757-899X/613/1/012051

[7] Gömze, L. A. – Gömze, L. N.: 2010 Építőanyag–JSBCM **62** (4) 98 http://dx.doi.org/10.14382/epitoanyag-jsbcm.2010.18

[8] Gömze, L. A. – Gömze, L. N.: 2017 IOP Conf. Ser.: Mater. Sci. Eng. **175** 012001 http://dx.doi.org/10.1088/1757-899X/175/1/012001

[9] Tihtih, M. et al: 2019 Építőanyag–JSBCM **71** (6) 190 https://doi.org/10.14382/epitoanyag-jsbcm.2019.33

[10] Buzimov, A. Y. et al: 2017 IOP Conf. Ser.: Mater. Sci. Eng. 175 012033 https://doi:10.1088/1757-899X/175/1/012033

[11] Kotova, O. B. et al: 2019 Építőanyag–JSBCM 71 (4) 125 https://doi.org/10.14382/epitoanyag-jsbcm.2019.22

[12] Apkaryan, A. et al: 2014 Építőanyag–JSBCM 66 (2) 38 http://dx.doi.org/10.14382/epitoanyag-jsbcm.2014.8

[13] Ibrahim, J. F. M. et al: 2019 IOP Conf. Ser.: Mater. Sci. Eng.613 012009 https://doi.org/10.1088/1757-899X/613/1/012009

[14] Ibrahim, J. E. F. M. et al: 2019 Építőanyag–JSBCM 71 (4) 120 https://doi.org/10.1088/1757-899X/613/1/012009

[15] Kurovics, E. et al: 2016 IOP Conf. Ser.: Mater. Sci. Eng. 123 012058 https://doi.org/10.1088/1757-899X/123/1/012058

[16] Kurovics, E. et al: 2019 Építőanyag–JSBCM 71 (4) 114 https://doi.org/10.14382/epitoanyag-jsbcm.2019.20

[17] Ibrahim, J. F. M. et al: 2017 Advanced Ceramics Progress 3 (4) 1

[18] Gömze, L. A – Gömze, L. N. 2009: Építőanyag–JSBCM **61** (2) 38 http://dx.doi.org/10.14382/epitoanyag-jsbcm.2009.7

[19] Ibrahim, J. F. M. et al: 2020 J. Phys.: Conf. Ser. 1527 012029 https://doi.org/10.1088/1742-6596/1527/1/012029

[20] Abdelfattah, M. et al: 2020 J. Phys.: Conf. Ser. 1527 012030 https://doi.org/10.1088/1742-6596/1527/1/012030

[21] Kurovics, E. et al: 2020 J. Phys.: Conf. Ser. 1527 012034 https://doi.org/10.1088/1742-6596/1527/1/012034

[22] Kurniati Ornam et al 2020 IOP Conf. Ser.: Mater. Sci. Eng. 797 012030 https://doi.org/10.1088/1757-899X/797/1/012030

[23] T. Woldu et al 2015 Chemical Physics Letters (625) 58-63 https://doi.org/10.1016/j.cplett.2015.02.020

[24] D. H. Park et al 2005 Ceramics International (31) 655–661 https://doi.org/10.1016/j.ceramint.2004.08.003

[25] J. F. Scott 2005 Materials Science And Engineering B: Solid-State Materials For Advanced Technology 120 (1-3), 6-12. https://doi.org/10.1016/j.mseb.2005.02.047

[26] A.H. Li et al 2008 J. Appl. Phys. 104 063526 https://doi.org/10.1063/1.2982396

[27] S. Komarneni et al 1999 Sol-Gel Sci. Techno. (15) 263 https://doi.org/10.1023/A:1008793126735

[28] M Tihtih et al 2020 J. Phys.: Conf. Ser. 1527 012043 https://doi.org/10.1088/1742-6596/1527/1/012043

[29] Kalim Deshmukh et al 2020 J. Phys.: Conf. Ser. 1527 012031 https://doi.org/10.1088/1742-6596/1527/1/012031

[30] W. J. Dawson 1988 Am. Ceram. Soc. Bull., 67 (10) 1673–78

[31] G. R. Fox et al 1990 J. Mater. Sci. (25) 3634 https://doi.org/10.1007/BF00575398

[32] J.A. Bland 1961 Acta Crystallographica, 14 (8) 875-881 https://doi.org/10.1107/S0365110X61002527

[33] J. Zhang et al 2009 Acta materialia 57(15) 4491-4499 https://doi.org/10.1016/j.actamat.2009.06.011

[34] M.R.A. Bhuiyan et al 2012 Int J Mater and Mech Eng (1) 21-24

[35] Y.Teraoka et al 1991 Chem.Lett 673

[36] E.A. Lombardo 1983 Journal of Catalysis 80(2) 340-349 https://doi.org/10.1016/0021-9517(83)90259-2

[37] M. Wu et al 1999 Journal of the American Ceramic Society 82(11) 3254-3256 https://doi.org/10.1111/j.1151-2916.1999.tb02235.x

[38] C.N. George, et al 2009 Materials characterization 60(4)322-326 https://doi.org/10.1016/j.matchar.2008.09.012

[39] F. G. S. Araujo et al 2000 Scr. Mater 43(5)447-452

Wenlock-Ludlow boundary sediments on Chernov uplift (Arctic region of Russia)

Vladimir A. Matveev ▪ Institute of Geology Komi SC UB RAS, Syktyvkar ▪ vamatveev@geo.komisc.ru

Tatiana M. Beznosova ▪ Institute of Geology Komi SC UB RAS, Syktyvkar
▪ beznosova@geo.komisc.ru

László A. Gömze ▪ Institute of Ceramics and Polymer Engineering, University of Miskolc, Hungary,
IGREX Engineering Service Ltd ▪ femgomze@uni-miskolc.hu

Abstract

The article presents the results of a study of Wenlock-Ludlow boundary sediments in the river Padimeytyvis basin at Chernov uplift using paleontological, lithological and chemostratic methods. The results of paleontological studies allowed attributing to the Wenlock the carbonate stratum of the upper part of the section along the stream Bezymjannyi and establishing Wenlock-Ludlow boundary only in the section of the river Padimeytyvis. The results of studying the isotope $\delta^{13}C_{carb}$ in Wenlock-Ludlow boundary sediments are also presented. In the upper part of the section along the stream Bezymyanny a positive C-isotopic shift of the curve which possibly marks the late Wenlock global biotic event of Mulde was observed.

Keywords: Ludlow, Wenlock, conodonts, brachiopods, Arctic region, Timan-Northern Ural region, isotope $\delta^{13}C_{carb}$.

Kulcsszavak: Ludlow, Wenlock, conodonta, brachiopoda, sarkvidéki régió, Timán-Észak-Urál régió, $\delta^{13}C_{carb}$ izotóp.

Vladimir A. MATVEEV
Scientific employee in the laboratory of stratigraphy at the N.P. Yushkin institute of Geology of the Komi SC UB RAS. Main fields of his research interest are stromatolite constructions of the Silurian of the Western slope of the Urals and the Chernov uplift. He is author of more than 30 scientific papers.

Tatiana M. BEZNOSOVA
Leading researcher at the laboratory of stratigraphy. Works at the N.P. Yushkin institute of Geology of the Komi SC UB RAS, Syktyvkar (Russian Federation). Main fields of her research interest are event stratigraphy, bio-chemostratigraphy, systematic, paleoecology and paleobiogeography brachiopods of the late Ordovician, Silurian and early Devonian Timan-Northern Ural region. She is author of 4 books and more than 150 scientific papers.

László A. GÖMZE
is establisher and professor of the Department of Ceramics and Silicate Engineering in the University of Miskolc, Hungary. He is author or co-author of 2 patents, 6 books and more than 300 scientific papers.

1. Introduction

The study of the stratigraphy of the paleozoic sediments of Chernov uplift began in 1921 by the Northern Scientific and Trade Expedition where G. A. Chernov worked. The results of the study of Silurian sediments and collections of fossil fauna are given in field diaries, thematic reports and published works by G. A. Chernov [1-3], S. A. Knjazev [4], A. I. Ljashenko [5], N. I. Timonin [6], A. I. Antoshkina, T. M. Beznosova [7], T. L. Modzalevskaya [8], T. M. Beznosova [9-11], P. Mannik, V. A. Matveev [12-13], N. V. Maidl [14], V. Y. Lukin [15]. In these works, the conditions for the formation of sediments composing the section, their age are considered, and their own stratigraphic dissection schemes are proposed. Issues of stratigraphy of Wenlock deposits in the Podymeityvis River basin have been reviewed repeatedly. A variety of conclusions about the age of Wenlock-Ludlow boundary stratum in the section of Chernov uplift testifies to the complexity of its structure and biostratigraphic dissection, as shown by our subsequent detailed studies. The history of the study of Silurian strata at Chernov uplift is given in publications [9-12].

In the sections of the Mikhailov-Vaigach structural-facies zone and the Timan-Northern Ural region the Wenlock-Ludlow boundary is determined with considerable relativity since it has an indistinct paleontological and lithological characteristic [16]. According to the stratigraphic scheme of the Urals, the regional Wenlock-Ludlow boundary between in the Timan-Northern Ural region is relatively established in a lithologically homogeneous member by the appearance of the ostracods Schreckia uralensis Abush. at the base of the Padimeytyvis horizon [17].

The newly conducted studies of sedimentation conditions of Silurian sediments at Chernov uplift made it possible to substantiate the stormy mode of sedimentation in Wenlock. A study of the collected fauna collections - the tabulate corals of brachiopods, ostracods, conodonts, vertebrates, the nature of changes in the behavior of isotope $\delta^{13}C_{carb}$ served to justify the Wenlock age of the Bezymyanny section and the Wenlock-Ludlow boundary in the section of the Podymeityvis River (*Fig. 1*). The established total thickness of Wenlock sediments at Chernov uplift is 300 m.
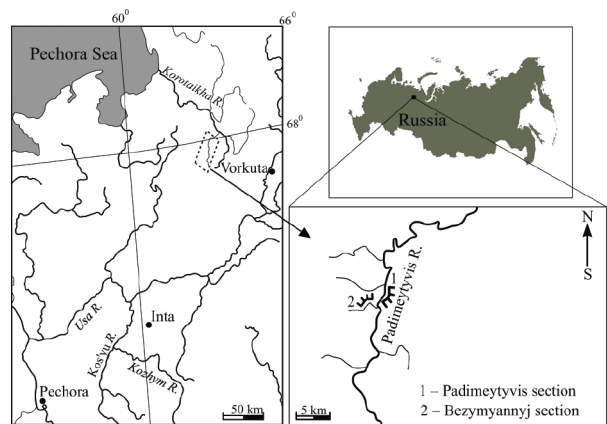
2. Geological setting

In the modern structural and tectonic plan, the studied section is located within the Pre-Ural foredeep in the Podymeityvis River basin at Chernov uplift (*Fig. 1*). It is customary to consider the Chernov uplift as a narrow near-fault horst-like structure, stretching in a sub-latitudinal direction from the Ajachyaginsky structure in the southeast to Sinkin Nose in the northwest.

On the whole, this is a near-thrust rootless structure formed as a result of the leaf-by-leaf stripping exposure in the cover of the Korotaikhinsky depression, confined to the incompetent Upper Ordovician member [6, 18].

3. Materials and methods

The material for this article was the collections of leaf-by-leaf samples collected by V. A. Matveev and P. Myannik during field work in 2010 and 2017. The collection of samples includes more than 53 samples with the remains of fossil macro- and microfauna, 44 samples for the isotope $\delta^{13}C_{carb}$.

The Wenlock section is opened along the Bezymyanny stream and continues with a gap on the river Padimeytyvis (left tributary of the Korotaikha River), where the Ludlow deposits are exposed. The studied Wenlock-Ludlow sections are located in the central part of the Chernov uplift in the Arctic part of the European North-East of Russia (*Fig. 1*). Organic remains were investigated by: T. M. Beznosova (brachiopods), P. Mannik (conodonts), V. Y. Lukin (tabulate corals), L. L. Shamsutdinova (ostracods), P. Mannik, L. V. Sokolova (conodonts), T. Märss (vertebrates). Lithological samples were studied by T. V. Maidl, stromatolites – by V. A. Matveev. Conclusions about the age of ostracods by A. F. Abushik [19] and stromatoporoids by O. V. Bogoyavlenskaya [7] were also taken into account.

The isotope $\delta^{13}C_{carb}$ in carbonate rocks was determined at the "Geoscience" of the Institute of Geology Komi SC UB RAS using a DELTA V Avantage mass spectrometer. The values of the isotope coefficients were determined in ppm (‰) according to the PDB standards NBS18 and NBS19 (TS-limestone) for carbon. The error in determining both coefficients did not exceed ± 0.1 ‰. The isotope $\delta^{13}C_{carb}$ was determined in 98 samples (sampling step 50 cm). The material for the isotope analysis was carbonate rocks, the least subjected to secondary transformations. Samples were obtained using a diamond drill with a diameter of 3.5 mm. Collections of fossil fauna remains are stored in the Museum named after A. A. Chernov of the Institute of Geology Komi SC UB RAS named after Academician N. P. Yushkin.

4. Results and discussion

The Wenlock-Ludlow boundary sediments are represented by the alternation of light brown to dark brown thin-layer limestones, platy with cracks of sediment drying, stromatolitic, clay, bioturbated limestones, containing numerous remains of ostracod shells, pelecipods, brachiopods, corals and other organisms.

The studied section thickness with a total capacity of 205 m was divided by us into six benches, three benches were identified along the Bezymyanny stream and three benches - along the Podymeityvis River. The first five benches belong to Wenlock, the sixth bench to Ludlow (*Fig. 2*).

5. Brief description of the section on the Bezymyanny stream

Unit 1 (thickness 36 m) is composed of interbedded brownish limestones and fine-grained and microgramed and limestones, dolomitic bituminous limestones, limestone with flat pebble conglomerate, ostracodic and brachiopodic limestones, which

also contain fragments of trilobites, gastropods, pelicipods. Defined: brachiopods *Spirinella nordensis* (Ljashenko), conodonts *Ozarkodina kozhimica* Melnikov, *Panderodus ex gr. greenlandesis* Armstrong, *Oulodus kozimicus* Melnikov, ostracods *Cytherellina aff. inornata* (Abushik), *Lichwinia silurica* (Neckaja). The upper boundary of the bench is carried out at the base of the first layer of stromatolite limestones.

Unit II (thickness 32 m) is represented by the interbedded brown, dark brown, fine-, micro-grained argillaceous limestones with silty shaly limestones, alternating with light lumpy spotted and micro-laminated microbial-algal and fenestrian limestones with leaf-by-leaf silty and argillo-dolomitic with lithoclasts and dessication fissures at different levels. A tectonic disturbance 1.8 m thick is observed in the lower part of the bench.
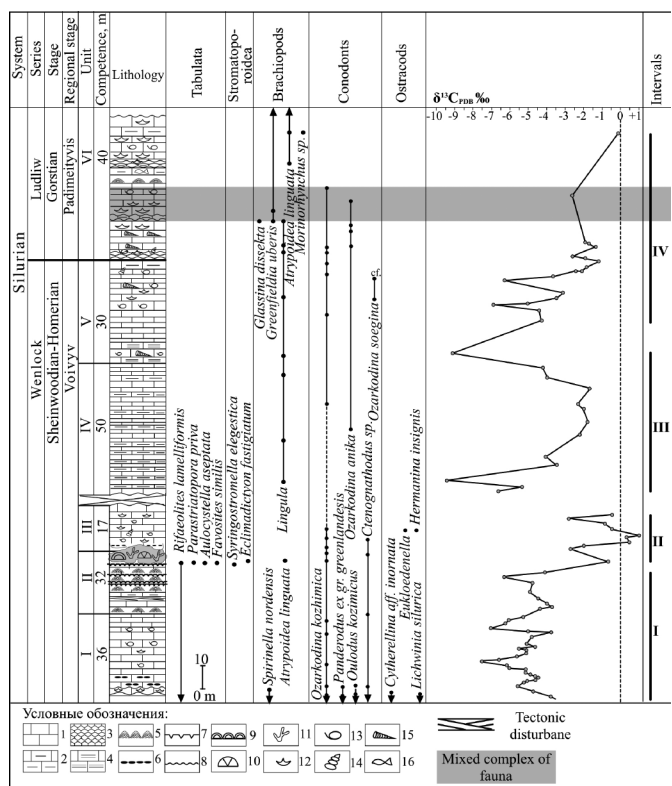

2. ábra A fauna és a δ^{13} izotópok eloszlása és a litológiai tulajdonságok a Padimeytyvis-folyó medencéjének Wenlock-Ludlow határmenti lerakódásaiban. 1-4 – mészkövek; 2 - agyagos; 3 - réteges; 5 - stromatolit; 6 - lapos-kavicsos konglomerátumok; 7 - sárrepedéses; 8 - hullámjelű; 9 - stromatoporoidea; 10 - tömeges táblás; 11 - elágazó táblás; 12– kagylók; 13 – haslábúak; 14 - csigák; 15 - férgek; 16 - gerincesek

Fig. 2 Distribution of fauna, isotopes $\delta^{13}C_{carb}$ and lithological features in the Wenlock-Ludlow boundary deposits in the Padimeytyvis river basin. 1-4 – limestones; 2 - clayed; 3 - laminated; 5 - stromatolitic; 6 – flat-pebble conglomerates; 7 – mud cracks; 8 - wave ripple mark; 9 - stromatoporoidea; 10 - massive tabulates; 11 - branched tabulates; 12– brachiopods; 13 - gastropods; 14 – orthoceratides; 15 - ostracods; 16 – vertebrates

In the bench, a stratum with organogenic structures is developed, which is represented by stromatolithic structures and coral-stromatoporate biostromes with a total thickness of 31 m (*Fig. 3, A*). In the lower part of this stratum, limestones with stromatolites of various morphological structures occur: bun-shaped, dome-shaped and beds, reaching a diameter of 55 cm and a height of 25 cm (*Fig. 3, B*). Similar Wenlock stromatolite structures are known in the north of the Urals, Chernyshev uplift, Dolgyi Island and Saaremaa Island in Estonia [8, 11, 15].
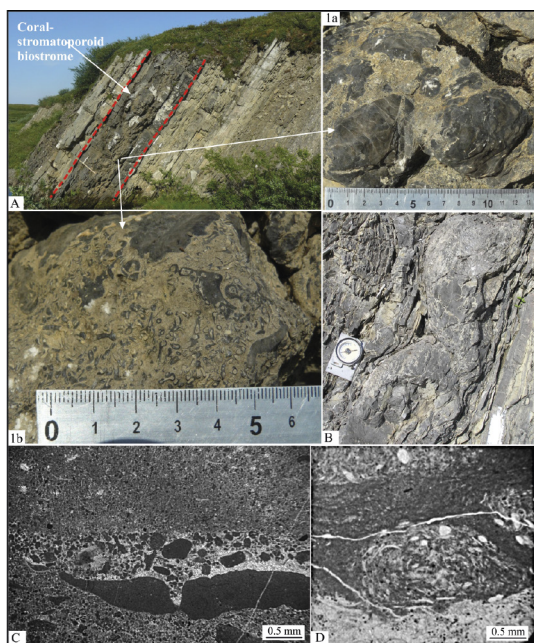
3. ábra   Korall-stromatoporoid biostróma (A (II egység)); 1a - stromatoporoid
kolónia); 1b - Aulocystella aseptata táblák (Barskaja, 1967); B - kupola alakú
stromatolit (II. egység); C - peloid mészkő lapos belső törmelékekkel (II.
egység); D - mészkő biomorf, subrodált kaotikus viharkúp (III. egység)

Fig. 3   Coral- stromatoporoid biostrome (A (Unit II)); 1a - colony of stromatoporoid;
1b - tabulates Aulocystella aseptata (Barskaja, 1967); B – dome-shaped
stromatolite (Unit II); C – peloid limestone with flat introclasts (Unit II);
D – limestone biomorphic with subrounded chaotic storm cone (Unit III)
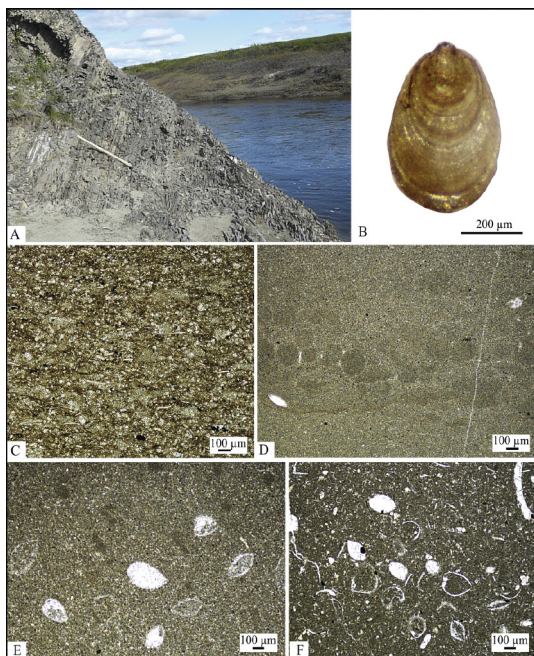
4. ábra   A Wenlock-Ludlow határlerakódások a Padimeytyvis folyó szakaszán.
A - Wenlock mészkő a mésztartalmú pala beékelődésekkel (IV. egység);
B - Lingula sp. kagylósférgek; C - pelitomorf mészkő vékony bioklasztikus
anyaggal (IV. egység); D - pelitomorf mészkő, bioturbált (IV. egység);
E - pelitomorf mészkő a Lingula sp. kagylók hossz- és keresztirányú héjával
(V. egység); Az F– mészkő bioklasztikus-pelitomorf jellegű, csontvázaival és
kagylók héjaival (V. egység).

Fig. 4   Wenlock-Ludlow boundary deposits in the section of the Padimeytyvis R iver.
A - Wenlock limestones with intercalations of calcareous shales (Unit IV);
B - brachiopod Lingula sp.; C - pelitomorphic limestone with thin bioclastic
material (Unit IV); D - pelitomorphic limestone, bioturbated (Unit IV);
E - pelitomorphic limestone with longitudinal and transverse shells of the
brachiopod Lingula sp (Unit V); F– limestone is bioclastic-pelitomorphic with
ostracods and brachiopod shells (Unit V)

Coral-stromatoporate biostromes with stromatoporoids *Syringostromella elegestica* Riab., *Ec. Fastigiatum* (*Fig. 3, 1a and 1b*), tubular tabulate corals *Aulocystella aseptata* Barskaja and dendritic tabulate corals *Riphaeolites lamelliformis* Klaamann lie above.

Thin-bedded limestones with ostracods and brachiopods *Atrypoidea linguata* (Bush) cover the biostrom; limestones with desiccation fissures and signs of indulation ripples lie above.

A similar structure of the Upper Wenlock section gap, comprising coral-stromatoporate and stromatolite biostroms, was described by D. K. Patrunov et al. on the Dolgyi island [20]. The conodonts *Ozarkodina kozhimica* Melnikov, *Ctenognathodus* sp. are defined in the bench. The upper boundary of the bench is the biostrome roof.

Unit III (thickness 17 m) is composed of brown and light brown fine- and medium-grained limestones with interbeds of limestone bioclastic, micro-layered, argillaceous. The lower part of the bench is composed of unsorted-detrital, biomorphic limestones, in which ostracods predominate, and interbeds of limestone with flat-pebble conglomerate (tempestites?) (*Fig. 3, C and D*) and signs of undulation ripples are also observed. Brown, micro-fine-grained, aphonite limestones with interbeds of unsorted-detrital limestones, mainly ostracodic, prevail above. Brachiopods *Atrypoidea linguata* (Bush), ostracods *Eukloedenella*, *Hermanina insignis* Abushik., conodonts *Ozarkodina kozhimica* Melnikov, *Ctenognathodus* sp. are defined.

The lithological structure features of this part of the Wenlock section (Benches I-III) suggest that its formation occurred in open shallow shelf conditions at low sea levels, with the prevalence of storm sedimentation and the general regressive orientation of the basin development [11].

Further, after a 100-110 m break, the section continues along the Podymeityvis River.

Unit IV (thickness 50 m) is composed of interbedded limestones of light brown pelitomorphic thin-bedded limestones (*Fig. 4, A*) containing a small amount of bioclastic material (*Fig. 4, C*), dark brown shaly limestones, argillaceous (1-5 cm) limestones and thin interbeds of calcareous argillaceous – shales. No visible fauna remains are found. When the rocks were dissolved on conodonts in the samples, the brachiopods *Lingula* sp. (*Fig. 4, B*) were found along with the conodonts of *Ozarkodina kozhimica* Melnikov.

Unit V (thickness 30 m) is composed of interbedded limestones of light brown micro-grained, thin-bedded to shaly with light brown massive, cryptocrystalline limestones, with semi-shelly fracture, and bioturbated limestones (*Fig. 4, D*). In the bench, single shells of brachiopods, gastropods, ostracods, and orthoceratide (1-5 cm) were found (*Fig. 4, E*). Brachiopods Lingula, conodonts *Ozarkodina kozhimica* Melnikov, *Ozarkodina anika* Viira et Einasto, 2003, *Ozarkodina cf. soegina* Viira et Einasto, 2003 were defined.

In the roof of this bench, the contact of thin-bedded limestones to shaly and bioturbated limestones is revealed. We consider this contact as the lithological Wenlock-Ludlow boundary. The paleontological boundary was drawn along the disappearance of the inarticulate brachiopods *Lingula* sp. and the appearance of the Ludlow brachiopods *Greenfieldia uberis* and numerous ostracods (*Fig 4, F*).

Unit VI (40 m thick) is composed of interbedded lumpy light brown limestones, thin-bedded limestones, dark gray bioclastic, pelitomorphic, bioturbated limestones with interbeds of dark brown shaly argillaceous. Four interbeds with stromatolithic dome-shaped structures of a diameter of 35 cm and a height of up to 15 cm are observed in the bench. On the weathered surface, it can be seen that the buildings are formed of a series of small dome-shaped and columnar structures, which are intergrown at the base, of a height of 7 cm and a diameter of up to 6 cm. Brachiopods *G. uberis*, *G. dissecta*, *M. attenuates*, *Atrypoidea linguata* Buch, *Lingula* sp., Wenlock-Ludlow conodonts *Ozarkodina kozhimica*, *Ozarkodina soegina*, *Ozarkodina cf. anika* (Viira et Einasto, 2003) and vertebrates *Thelodus visvaldi* Karatajūtė-Talimaa et Märss, 2002, are defined in the bench limestones.

6. Biota of Wenlock-Ludlow boundary sediments

The sea basin level increase in the late Wenlock (Sheinwudian) contributed to the taxonomic diversity of the biota. The benthic communities were based on the brachiopods represented by the *Arypoidea linguata* atrypids and the first in Silur speririfirds of the *Spirinella nordensis*, which are known in Wenlock of the Dolgy and Gotland Islands, in Great Britain, Bohemia, Mongolia, Southern China, in Llandovery and Wenlock of North America and Ludlow of Estonia. Along with brachiopods the ostracods *Hermanina insignis* (Abushik), *Eukloedenella grandifabae* Abushik, as well as gastropods, pelecipods, coral and stromatoporoid communities that formed the biostromes [11, 19] were developed at that time. The gradual shallowing of the basin, the development of stromatolith-forming organisms negatively affected the existence of the Spirinella brachiopods belonging to the third benthic complex (B.C. 3) and *Atrypoidea* belonging to B.C. 2 [21]. The increase in stromatolith interbeds observed upstream of the section, as well as desiccation fissures, indicates a progressive regression, as a result of which stromatoporoids, ostracods, pelecipods, ostracods disappeared.

Wenlock deposits (thickness about 100 m), which are opened in the section along the Podymeityvis River, represented by thin-bedded, argillaceous limestones, do not contain visible fauna remains. When dissolving conodonts samples in this strata, the valves of inarticulate brachiopods Lingula belonging to B.C. 1 were defined.

Transition from Wenlock to Ludlow in the section of the river Padimeytyvis is recorded by the change of light brown, thin-bedded, argillaceous limestones containing Wenlock conodonts complex and *Lingula* brachiopods with a depleted composition of benthic fauna to lumpy argillaceous limestones of massive appearance enclosing the *Greenfieldia uberis* brachiopod community. The paleontological Wenlock-Ludlow boundary is determined by the updated fauna composition (brachiopods, ostracods, vertebrates) in lumpy argillaceous limestones that compose the lower part of the Padimeytyvis Ludlow horizon. Limestones with brachiopod shells *Glassina dissecta* T. Modz., *Morinorhynchus attenuata* (Amsd.), *Atrypoidea linguata* (Buch), *Greenfieldia uberus* T. Modz. form distinct marking layers, which are traced at the Ludlow base on the Western slope of the Polar and Northern Urals, on Chernyshev uplift and numerous well sections of the Timan-Pechora oil and gas province [10].

As for the vertebrates, the remains of the vertebrates *Thelodus visvaldi* were discovered in the section, which until now were known only on the Severnaya Zemlya [22].

The section interval of Wenlock-Ludlow boundary sediments with a thickness of 13.7 m is characterized by a mixed complex of the Ludlow benthic fauna and the Wenlock complex of conodonts. In *Fig. 2*, this section interval is highlighted in gray. Examples of joint finds of fauna remains of different ages are known at the Llandovery-Wenlock boundary at the Chernov uplift, as well as at the Ludlow-Pridoli boundary in the section of the western slope of the Subpolar Urals [23, 24, 11].

7. C_{carb} Isotope Analysis

The results of the isotope analysis, sequentially tied to the intervals of the section, showed the possibility of identifying four intervals with characteristic isotopic values that are consistent with paleontological and lithological data (*Fig. 2*).

Isotope characteristics of carbonates of the Wenlock-Ludlow boundary deposits in the river Padimeytyvis basin showed that in Wenlock $\delta^{13}C_{carb}$ values are in the range from –9.51 to 1 ‰, and in Ludlow from –3 to 0 ‰.

In interval I, composed mainly of pelitomorphic, bio-, lithoclastic, stromatolitic limestones, the isotope $\delta^{13}C_{carb}$ is characterized by negative values. The average value of the isotope coefficient for carbon is $\delta^{13}C_{carb}$ –5.15 ‰. Up the section, the isotope $\delta^{13}C_{carb}$ has wave-like oscillations; first, the carbon values fall from –4.35 to –7.5 ‰, which then increase to –3.8 ‰ and fall to –7.0 ‰.

In interval II, a sharp weighting of the isotope $\delta^{13}C_{carb}$ is observed, which begins at the base of the coral-stromatoporate biostrome (bed 101) $\delta^{13}C_{carb}$ –6.3 ... –0.6 ‰ and continues to the very top of the section, where it reaches maximum values + 1 ‰ (bad 109). The average isotope $\delta^{13}C_{carb}$ value for this interval is –1.18 ‰. A sharp shift of the isotope curve towards positive $\delta^{13}C_{carb}$ values may correspond to the Early Wenlock biotic and isotopic Mulde event. This event is characterized by the extinction of the graptolite and conodont fauna, as well as a double positive excursion of carbon isotopes, which lies in many sections of the world [25-28].

In interval III, the average value of the isotope coefficient for carbon is –4.48 ‰. The interval is characterized by two abnormal negative values $\delta^{13}C_{carb}$ –9.51 ... –9.10 ‰.

Interval IV. The average value of the carbon isotope coefficient for this interval is $\delta^{13}C_{carb}$ –2.98 ‰. In the lower part of the interval, two peaks of negative values of carbon isotopes –6.29 ... –6.93 ‰ are recorded. Above the section, the interval is characterized by a gradual weighting of the isotope $\delta^{13}C_{carb}$ –6.93...–0.13 ‰, which sets the trend in the positive direction of the curve.

Considering the extremely shallow deposits of the studied Wenlock-Ludlow boundary deposits, it can be assumed that the isotope-facilitated fresh water from the continent saturated with dissolved soil carbon dioxide during climate humidization periods and a corresponding increase in terrigenous runoff could influence the isotope values changes. A sharp weighting of the isotope $\delta^{13}C_{carb}$ at the base of the coral-stromatoporate biostrome, unlike the lying above and below values, may indicate a change of water in the sedimentation basin from desalted to

normal marine [29, 30]. Such an effect is also associated with an increase in the biological productivity of the reservoir, due to warming and an increase of the sea level, which is correlated with lithological data (sequential change of layers with stromatolithic structures to coral-stromatoporate biostroms and then to limestones with diverse benthic fauna). Sharp spasmodic shifts of the isotonic curve in the studied section indicate significant changes in the characteristics of the medium of Wenlock-Ludlow boundary sedimentation in the Timan-Northern Ural Sea Basin.

8. Conclusions

The conducted studies supplemented the paleontological and sedimentological characteristics of Wenlock-Ludlow boundary deposits. For the first time, Wenlock-Ludlow boundary deposits received paleontological and chemostratigraphic evidence. The established thickness of Wenlock sediments at the Chernov uplift is 300 m. Two intervals were traced in the boundary deposits in which the brachiopod communities change from benthic complex 1 in Wenlock to benthic complex 2 in Ludlow. The established anomalous excursions of carbon isotopes in the section can serve as reliable chronostratigraphic benchmarks for regional and global correlation of Wenlock sections. The results of the study confirm and complete the conclusions of G. A. Chernov on the links of the Timan-Northern Ural Sea Basin with the Baltic and Western Europe basins.

Acknowledgements

References

[1] Chernov, G. A. (1964): Silurian deposits of the Chernov uplift // Doklady Earth Sciences. SSSR, pp. 843–846.

[2] Chernov, G. A. (1966): Silurian stromatolites of the Chernov uplift (Bolshezemelskaya Tundra). Stratigraphy and Paleontology of North-West European Region of the USSR. Moscow, Leningrad: Nauka, pp. 90–105.

[3] Chernov, G. A. (1972): Paleozoic of the Bolshezemelskaya tundra and the prospects of its oil and gas bearing sections. Moscow: Nauka, 318 p.

[4] Knyazev, S. A. (1965): Silurian Deposits of the Central Part of the Chernov Uplift // Materials on the Geology and Minerals of Northeastern Eurasia, USSR. Syktyvkar, No. 5. pp. 112–120.

[5] Lyashenko, A. I. (1964): New species of Devonian brachiopods of the Russian platform and the Western slope of the Urals // Fauna of the Paleozoic of the Volga-Ural region of the oil and gas province. Moscow: Nauka, pp. 3–57.

[6] Timonin, N. I. (1998): Pechora Plate: History of Geological Development in the Phanerozoic. Ekaterinburg, 240 p.

[7] Antoshkina, A. I. – Beznosova T. M. (1988): New data on stratigraphy Wenlock deposits of the Bolshezmelskaya tundra. Bull. MOIP. Otdelenie geo, Vol. 63. No. 6. pp. 32–39.

[8] Modzalevskaya, T. L. (1980): Some questions of stratigraphy of Silurian deposits of the Bolshezemelskaya tundra // Annual VPO. L., Vol. 23. pp. 299–304.

[9] Beznosova, T. M. (1994): Biostratigraphy and brachiopods of the Silurian of Northeastern European Russia. St. Petersburg: Nauka. 128 p.

[10] Beznosova, T. M. (2008): Brachiopod communities and biostratigraphy of Upper Ordovician, Silurian and Lower Devonian of North-Eastern margin of Baltia paleocontinent. Ekaterinburg. 218 p.

[11] Beznosova, T. M. – Mannik, P. – Maidl', T. V. – Lukin, V. Yu. – Matveev, V. A. (2014): Depositional conditions and biota in the Llandovery-Wenlock boundary interval (Chernov uplift). Vestnik of Institute of Geology of Komi SC UB RAS, No. 3. pp. 14–18.

[12] Matveev, V. A. (2011): Wenlock stromatolitic buildups from the Chernov uplift: main morphotypes, microstructure. Vestnik of Institute of geology of Komi SC UB RAS. No. 11, pp. 2–5.

[13] Matveev, V. A. (2017): Ultrastructures of stromatolites from the Wenlock of Chernov uplift. Doklady Earth Sciences, Vol. 474, No. 2, pp. 206–209. https://doi.org/10.1134/S1028334X17050142

[14] Lukin, V. Yu. (2014): Systematic position of the species Syringoporinus aseptata Barskaja, 1967 from Silurian deposits of Chernov uplift (Bolshezemel`skaya tundra. Syktyvkarskij paleontologicheskij sbornik RAN. pp. 129.

[15] Majdl, T. V. (2013): Flat pebble conglomerates – storm sediments of the Lower Paleozoic of the Pechora sedimentary basin. Vestnik of Institute of geology of Komi SC UB RAS, No. 4, pp. 2–6.

[16] Nekhorosheva, L. V. – Patrunov, D. K. (1981): Greben' stage of the Island Vaygach-Novaya Zemlya region]. Sov. geologiya, No. 4, pp. 80-85.

[17] Explanatory note to Ural stratigraphic maps (Antsygin N.Ya. Ed) (1994): Ekaterinburg, 95 p.

[18] Yudin, V. V. (1994): Orogenesis of the Northern Urals and Pay-Khoy areas. Ekaterinburg: "Nauka", 286 p.

[19] Abushik, A. F. (2000): Silurian-Earliest Devonian ostracode biostratigraphy of the Timan – Northern Ural Region // Estonian Acad. Sci. Geol, Vol. 49, No 2. pp. 112–125.

[20] Patrunov, D. K. – Shurygina, M. V. – Cherkesova, S. V. (1980): The Silurian and Lower Devonian of the Dolgiy Island. Silurian and Lower Devonian Deposits of the Dolgiy Island. Sverdlovsk, pp. 3–26.

[21] Boucot, A. J. (1975): Community extinction and rate control. Amsterdam. P. 1–427.

[22] Karatajute-Talimaa, V. – Märss, T. (2002): Upper Silurian thelodonts from Severnaya Zemlya Archipelago (Russia). Geodiversitas, 24 (2), pp. 405–443.

[23] Beznosova, T. M. – Matveev, V. A. – Sokolova, L. V. (2019): Upper Ludlowian-lower Pridolian stratigraphy, carbon isotope of the Timan-Northern Urals region // Építőanyag. Vol. 71, No. 1. pp. 24-37. https://doi.org/10.14382/epitoanyag-jsbcm.2019.5

[24] Kanev, Bronislav I. – Beznosova, Tatiana M. – Matveev, Vladimir A. – Gömze, László A.: Environment changes at the Ludlow and Pridoli boundary (Subpolar Urals) // Építőanyag, 2017. vol. 69, no. 4. P. 132-133. https://doi.org/10.14382/epitoanyag-jsbcm.2017.24

[25] Kaljo, D. – Kiipli, T. – Martma, T. (1997): Carbon isotope event marker sthrough the Wenlock-Pridoli sequence at Ohesaare (Estonia) and Priekule (Latvia). Palaeogeography, Palaeoclimatology, Palaeoecology, 132, pp. 211–223. https://doi.org/10.1016/S0031-0182(97)00065-5

[26] Calner, M. – Eriksson, M. E. (2006): Silurian research at the crossroads. GFF 128(2), pp. 73-74. https://doi.org/10.1080/11035890601282073

[27] Cramer, B. D. – Kleffner, M. A. – Saltzman, M. R. (2006): The Late Wenlock Muldepositive carbon isotope ($\delta^{13}C_{carb}$) excursion in North America. GFF 128, pp. 85-90. https://doi.org/10.1080/11035890601282085

[28] Munnecke, A. – Calner, M. – Harper, D. A. T. – Servais, T. (2010): Ordovician and Silurian seawater chemistry, sea level, and climate: a synopsis. Palaeogeogr. Palaeoclimatol. Palaeoecol. 296, pp. 389–413. https://doi.org/10.1016/j.palaeo.2010.08.001.

[29] Yudovich, Ya. E. – Ketris, M. P. (2010): Relationships of carbon isotope in the stratosphere and biosphere: Four scenarios, Biosfera, 2010, Vol. 2, No. 2, pp. 231-246.

[30] Yudovich, Ya. E. – Ketris, M. P. (2011): Geochemical Indicators of Lithogenesis: Lithological Geochemistry), Syktyvkar: Geoprint, 742 p.

Insights into the applicability of the X-Ray phase quantification supported by SEM for the rock-forming silicates minerals in the basaltic lava flows

Irina M. Gembitskaya ▪ Saint Petersburg Mining University,
Russian Federation ▪ gembitckaia_im@pers.spmi.ru

Elena L. Kotova ▪ Saint-Petersburg Mining University, Russian Federation ▪ kotova_el@pers.spmi.ru

Ilnur A. Abdrakhmanov ▪ Saint-Petersburg Mining University,
Russian Federation ▪ ilnur_01_95@mail.ru

Emese Kurovics ▪ Institute of Ceramics and Polymer Engineering,
University of Miskolc, Hungary ▪ fememese@uni-miskolc.hu

László A. Gömze ▪ Institute of Ceramics and Polymer Engineering, University of Miskolc,
IGREX Engineering Service Ltd, Hungary and Tomsk State University, Russia ▪ femgomze@uni-miskolc.hu

Irina M. GEMBITSKAYA
Is a Leading Researcher of Saint Petersburg Mining university. Author and co-author of more than 90 articles.

Elena L. KOTOVA
is a Scientific director of the Mining museum of the Saint-Petersburg Mining university. Author and co-author of chapter in book, 1 patent and 32 articles. The member of the Russian Mineralogical Society, Oil and gas historical Society of Russia.

Ilnur A. ABDRAKHMANOV
Is a Postgraduate Student department of Mineralogy. Author and co-author 2 articles. The member of the Russian Mineralogical Society.

Emese KUROVICS
is graduated from the University of Miskolc, Department of Ceramics and Silicate Engineering as a material engineer, where she continues her study as PhD student under supervision of Prof. L. A. Gömze.

László A. GÖMZE
is establisher and professor of the Department of Ceramics and Silicate Engineering in the University of Miskolc, Hungary. He is author or co-author of 2 patents, 6 books and more than 300 scientific papers.

Abstract

The authors present their results obtained from the study of the magmatic rock-forming mineral phase-relations. In the study a number of standard and modern instruments were used for sample analyses. These include the X-Ray Diffraction, Scanning Electron Microscopy, X-Ray microprobe analysis and laser-granulometry analytic method. A combination of these instruments is considered very robust in the study of magmatic mineral-phases. The dataset obtained through the use of X-Ray Diffraction in combination with a corrected calibration on the mono-mineral fractions plays a critical role in comparing series of volcanic basalts. This approach was chosen for comparison studies of the volcanics due to its optical precision in determining modes and petrographic characteristics of the basaltic rocks. This study has used basaltic rocks from the modern volcanic eruptions of the Tolbachik region in the Russian Federation. Studies of other additional basaltic rocks were conducted from 10 samples which represents the Etna eruption which occurred in 2001. This enabled us to constrain the diversity in the nature of basaltic rocks of these two events.

Key words: basaltic lava flows, Etna, SEM, Tolbachik, X-Ray Diffraction

Kulcsszavak: bazaltos lávafolyások, Etna, SEM, Tolbachik, röntgendiffrakció

1. Introduction

The Tolbachik volcanic event represents one of the few volcanic events which erupted the northern section of the Russian in the early Mesozoic period. One of the key features of basaltic melts is its micro-heterogeneous structure. Its transformation is the basis for different mobility of melt components, the behavior of volatiles, and process of polymerization and structural-chemical peculiarities of the silicates crystals. Methods of study of phase transformations are shown in [1–5]. This paper studies the phase-relations of the recent basaltic eruptions and intends to provide a comprehensive approach that combines macro-(X-ray diffraction) and micro-/nano- (SEM) exploratory methods for spatial-temporal reconstruction of pre-eruptive dynamics. Based on the early study of rhyolites which was pioneered by Tatlock [6], the XRD application in quantifying mineral phases of these and other rock types has proven to be robust. These included the study of granites, volcaniclastic inputs into marine sediments, mudstones and carbonate rocks [7, 8].

The application of these methods involves the assessment of quantitative ratios between minerals and their fine features. Our study further compares the phase composition of samples with different quenching rates (degree of crystallinity): scoria, volcanic bombs, surface crusts or thin lava plates, lava, selected in a liquid state and hardened in air or water and lava, and those which were slowly cooled in the stream which shows a diverse phase-relation with similar chemistry.

The Rietveld method which was proposed by H.M Rietveld was applied herein to determine the main phase-proportions: olivine, pyroxene, plagioclase and volcanic glasses from 70 basaltic samples of the Tolbachick volcanic vent.

The Rietveld method is a widely accepted method due to its whole-pattern fitting approach instead of single-peak analysis. The main advantage is that it can minimize or eliminate the errors arising from preferred orientation, particle statistics, microabsorption, peaks overlapping, and detection of amorphous phase and trace phases. Various amount of glass and crystals with broad isomorphism requires a different approximation [9]. The main conclusion was that, if amorphous material is present, quantitative results could not be obtained directly. The current study is devoted to similar basalt ranges with the smaller amount of olivines. The task requires mechanism of finding a log-linear response the diffractions maximums intensities to phase concentration and the sample-preparation process optimality (various grinding, pressing, mounting).

2. Geological setting

Tolbachik is situated within the central Kamchatka depression, forming part of the Kluchevskoy group of volcanoes, the most active-volcanic vent in the Kamchatka arc. it encompasses the southern part of the Klyuchevskaya Volcanic Group, which is located within the Central Kamchatka Depression. The group is well-known to be one of the most productive and diverse subduction-related volcanic area on Earth with compositions of the erupting magmas ranging from basalt to dacite [10]. The volcanism of the group is driven by the subduction of the Pacific Plate under the Okhotsk microplate with an average convergence rate of 9 cm/yr. The unusually high rate of magmatic production is likely related to both great subduction rates and the proximity of the group to the corner of the Pacific Plate. Tolbachik is a comparatively well-studied volcanic complex in central Kamchatka. Early studies which were conducted in the complex dates back to the 18th century.

Piip [10] made a comprehensive study on the general geological features of the volcano and its eruption. His study covered the aspects of various basaltic melts. A large volume of geological, geochemical, and geophysical data was also collected during the 1975/1976 volcanic eruption famously known as 'The Great Tolbachik Fissure Eruption' [11].

The ASI shows the structural-chemical behaviour of the melt components as the molecular relationships Al_2O_3 (Al in tetrahedral position as Si) to net-forming cations (usually the alkaline and alkaline earth elements) ASI $=Al_2O_3/$ (Na_2O+K_2O+ CaO). The Tolbachik volcanic series primarily comprises of two rock types: middle-K, high-Mg (Mg/Al: 2,1; ASI: 0,45) basalts and high-K, high-Al (Mg/Al: 0,45; ASI: 0.8) basalts. The two basaltic series are composed of different major element concentrations with the greatest variation observed in Mg and Al contents. General regularities of changes in the chemical composition of the fissure eruptions in the Tolbachik zone are: the two extreme types of basalts which differ primarily in the content of Mg and Al. Besides that Ni, Co, Cr behaves like Mg and P, Ti, Na, K, Rb, Li like Al.

The high-Mg basalt was erupted during the 1941 activity, both types as well as the intermediate were erupted in the 1975–76, the high-Al basalt was erupted during the 2012–2013. The high-Al basalts were volumetrically dominant during the Holocene and comprise of more than 90% of the erupted material in Tolbachik volcanic zone. The main rock-forming minerals in all the volcanic lavas along the fault zone constituted of Ol, Cpx and Pl.

The basalts and intermediate rock types are predominantly characterized by isomorphic phases: Ol varies from Fo_{83-90}, Cpx is diopside, diopsidic augite, augite with Mg_{66-88}, and Pl is labradorite with An_{80-44}.

3. Sampling

The rock materials of the 3 volcanic eruptions which occurred in Tolbachik area around 1941, 1975-1976, 2012-2013 were sampled. The erupted materials were sampled from the lava flows, volcanic bombs and, where possible, from scoria. The lapilli and bombs were collected, and a precautionary measure was taken into account during the sampling; where early pyroclastic materials were chosen in areas which are free from contamination by recent eruption.

Lavas were sampled in line with date and duration of their outpouring as well as the maps of lava fields showing the 1941, 1975-1976 and 2012-2013 flow units [10, 11]. The GPS coordinate database (IVS FEB RAS, Kamchatka) was of great assistance during the sampling of the 2012-2013 volcanic event. These events indicate similar features and spread along the same linear fault zone, although with variable intensity, duration, and various stages of differentiation [12]. The samples were collected along the lava flows from intermediate parts of lava flows using a sampling grid of approximately 200-400m between points. Where possible, samples were taken from the basal zone (near bottom), from lava core and near the upper lava crust. Some of the samples: 6SBliq, M1912, M2512 were collected in a liquid state, the water or air quenched. Most of samples were collected after the lava had naturally cooled.

To test the approach applicability to basaltic products of other volcanoes, ten samples were collected from 2001 Etna lava flows (ASI: 0, 55-0, 6; Mg/Al: 1, 05-0, 75). They were chosen because their quantification in optical mode had been previously studied by [13]. By the same token, various ranges of basaltic compositions have been encompassed.

4. Sample preparation procedures

Many mistakes can be minimized by adhering to proper sample preparation procedures, particularly in ensuring homogeneity of powder composition and grains sizes. To get optimum results these conditions were necessary: totally homogeneity over a range of 1 μm (range), constant particles size, and absence of preferred orientation (texture), and also the lattice strain. The preparation of the suitable powders was done after choosing an optimal particles size. The rock powder was prepared using a five-minute grind in vibration mill Retsch Mixer Mill MM301 with ZrO_2 ball and further grind in agate mortar to reach range of the particle's sizes from 1 to 5 μm. The grinding time was chosen in experimental procedure, including measurements of grains sizes (*Fig. 1b*) and intensities of analytical X-ray peaks (*Fig. 1c, 1d*) ten minutes via (*Fig. 1a*). The optimal grinding time in agate mortar was 35 min. The powders were examined by using SEM and the laser scattering particle size distribution analyzer Horiba LA960.
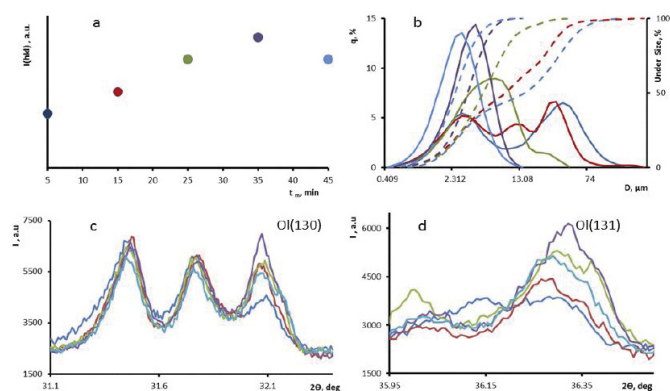
1. ábra *A porrészecskék optimális méretének meghatározása a mintadarabon, minimális olivin-tartalommal*

Fig. 1 *Powder particles optimal size determination on the specimen with min olivine content*

5. Analytical procedures

The prepared lava samples and scoria were analyzed using X-ray diffractometer XRD6000 and processed under software control. X-ray powder diffraction data was provided with diffractometer, with Cu Ka radiation and Ni filter. An amount of 5 wt.% reference germanium standard material was added to the powder to calculate exactly the set of dhkl. Spectra were taken in the 2h-range 5–70, using 35 kV, 45mA, speed 0.015deg/min, pitch 0.008 deg., present time 32 sec a stepsize of 0.02, a counting time of 5 s per step, divergence and antiscatter slits of 1 and receiving slit of 0.2 mm.

The powdered samples were loaded on a sample holder by mixing thoroughly with ethanol. At first the two different cuvettes were used with front or side loading the powder to examine influence of grain orientations, and then lots of sub-samples (3-5pieces) were prepared and measured in order to arrive at a result which is indeed representative for the variable mineral composition. Analytical steps included: the measurement ranges being chosen, checked or refined for every new suit of samples; checking the stability of the X-ray generation; choosing scan speed 0.5 degree/min for common measurements and 0.03 degree/min for the olivine peaks (130), (131) and for the Cpx peaks (610), (131). The XRD peaks profiles varied according to glass ratio, grains sizes, isomorphism, macrostrains, and transformations of the minerals. Every sample measurement was repeated 3 times to check reproducibility. We applied mixtures from monomineral fractions (by washing of the crystals from the glass, using a special technique of HF flushing) and volcanic glass for calibrations. They were examined by using SEM and the laser scattering particle size distribution analyzer Horiba LA960 before using them as reference standards. It is well known, that the laser particle size analyzer doesn't measure about 5% smallest grains as well as 5% the biggest grains and doesn't notice complicated shape of particles. In this case a SEM provides quickly to determine what kind of problem does arise, if the sample is not ideal. It's very convenient to do the control of powder and specimen in SEM with COMPO signal and in low vac mode.

The powders of Ol, Px, Pl and glass were weighed, with a designed mass ratio of 10:30:40:20; 5:20:55:20; 0:40:40:20; 0:35:55:10; 10:30:50:10 respectively. The above powders were subsequently mixed and homogenized by hand for 30min in an agate mortar. Finally, they were loaded on to the holder for XRD measurement. Those mixtures were prepared and then underwent XRD tests by triplicate, but XRD patterns didn't show significant differences. Inner standard substance has been added in each powder to control the crystal lattice parameters. This operation allowed observing wide range of silicate isomorphic substitutions that was especially useful for olivine.

6. Processing and results

Almost all the analyzed samples show similar mineralogical composition decides the samples directly from the lava from, which compose kaersutite. The most complicated analytical peak was (130) by Ol. The low quantity of Ol, the peak overloading by fluctuation of dhkl from 2.7991 to 2.7700 Å needs special conditions (*Fig. 2*).

To find out the reasons for the peak profile transformations, we analyzed the olivine composition by X-ray and XRMA data (*Table 1*).
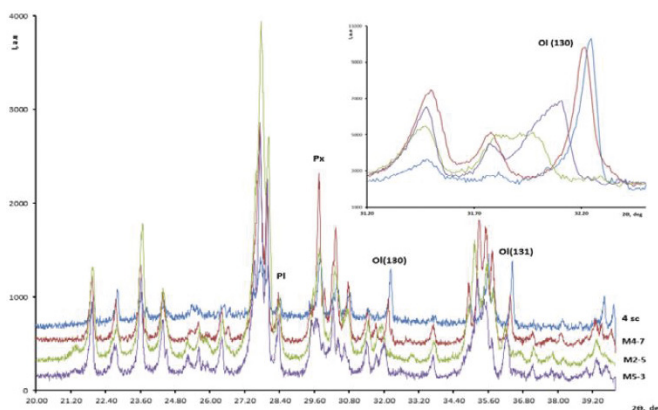
2. ábra A fázis összetételében leginkább különböző minták diffraktogramjai (analitikai diffrakciós maximumokkal)
Fig. 2 The examples of diffractograms of the samples most differing in phase composition (analytical diffraction maxima indicated)

Sample	Fo% (XRD average)	Fo%(XRMA) center of crystal/ rim of crystal	
		size>700µm	Size<700µm
4sc	89	89/90/82	77/87
4B	86.5	89/81	83/81
4-9	85	88/77	83/81
4-6	80	89/81	88/77
4-7	78	90/93/81	83/77
6NB	87	89/81	88/77
6N-Bsc	79	89/79	77
6SB-liq	73	77	77/69
6SB1	73	75/67	71
6SB2	71	75	71
M2-5	49	49	50/49
M1-8	72	73/67	72
M19-12-liq	72	71/73/67	70/67
M25-02liq	73	–	72/69
M5-3	68	73	67
p1-1	70	79/73	78/67
p2	72	–	73/70
p3a	73		
p4	77	79/78	81/72
p6	75	81/76	80/72
p5	71	78	79/72

1. táblázat Ol-ben az XRD és XRMA módszerrel mért Fo% összehasonlítása
*Table 1 Comparing Fo% in Ol measuring by XRD and XRMA*

For examples BSE (COMPO) images of olivine crystals from the early melt crystallization appear to have a normal zoning pattern that shows dark cores surrounded by bright rims, implying that Fe increases towards the rim. However, the higher resolution images show that between the cores and the rims there is a zone of higher Fo and Ni content. The main mechanism of the Pl and Cpx crystals growth is agglomeration from nano-and/or micro-particles. The sizes of these aggregates are from 0,N mkm to N mm. When the lava spreads over a larger distance (km), the redox conditions destroy the olivine structure and produce the micro inclusions of Px+Mgt. All of these processes

(*Fig. 3*) lead to broadening of the diffraction maxima. This can result in difficulties when correcting the intensity measurements. It is therefore necessary to use more reliable combination of calibration from mixtures of monomineral phases and control of the degree of heterogeneity from SEM images

The XRD semi-quantitative analytic results are presented in *Fig. 4*. Some of the important phase-ratios are calculated. The phase behaviour according to optical and X-ray data differ, especially in the case of growth by agglomeration with down density (gaps between crystallites may be up to 50%).
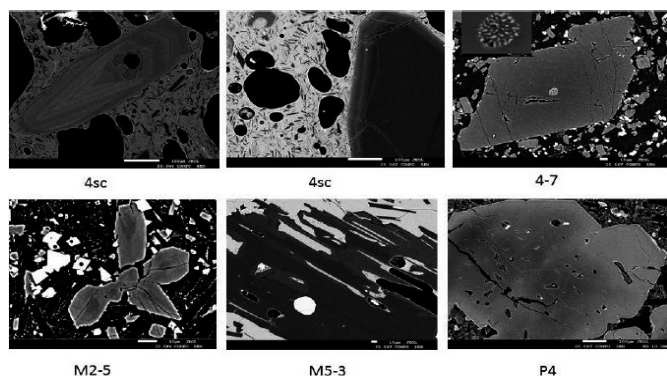
3. ábra A SEM-képek a bazaltok és ásványok különbözőségéről, heterogenitásáról
Fig. 3 The SEM images in composition contrast showing heterogeneity of basalts and minerals
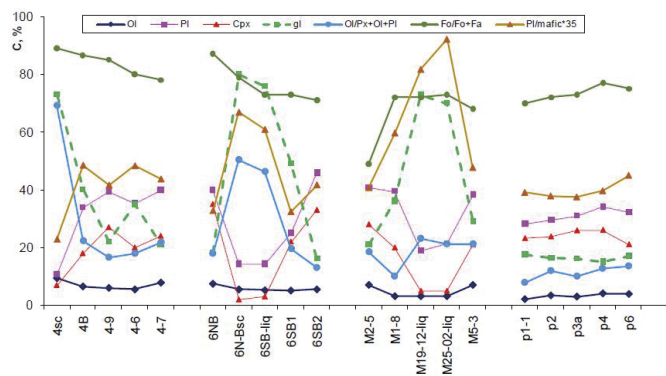
4. ábra A szilikát ásványi anyagok tartalmának, arányuknak és az Mg-tartalomnak az Ol-ben történő számszerűsítése
Fig. 4 Quantification of the silicate minerals content, their ratios and the Mg-content in Ol

7. Conclusions

On the basis of a comparison of the phase composition of these samples, we clarify the transformation of the mineral phases due to crystallization and/or dissolution, as well as the diffusion of the components in the final stage of rock crystallization. The main observable patterns are:

1) A decrease in the amount of olivine in front of lava flow which is attributable to redox conditions

2) The similarity in phase composition and the relative stability of the phase ratios, while the magnesian differences are sensitive to the cooling conditions: temperature, spreading rate and quenching rate.

3) A direct correlation between the crystallinity of the samples and the content of plagioclase and clinopyroxene. The mass crystallization of clinopyroxene, titanomagnetite, plagioclase occurs during the outflow of lava to the surface, appearance kaersutite in front of lava flow

4) Increasing content of Fe in olivines in some of lava flows along with small oscillations/fluctuation of the common olivine content in basalt.

When the ratios of the mineral phases are calculated according to the optical method it is impossible to take into account the real microstructure. Development work is required to study every basaltic series, but testing showed that the correct mineral ratios are achieved by XRD- means. The usefulness of this approach is to reduce the data processing time and amount of errors by petrological calculations in the routine rock study in microscope.

References

[1] Kotova, O. B. – Shushkov, D. A. – Gömze, L. A. – Kurovics, E. – Ignatiev, G. V. – Sitnikov, P. A. – Ryabkov, Y. I. – Vaseneva, I. N.: Composite materials based on zeolite-montmorillonite rocks and aluminosilicate wastes Építőanyag – JSBCM, Vol. 71, No. 4 (2019), 125–130. p. https://doi.org/10.14382/epitoanyag-jsbcm.2019.22

[2] Razmyslov, I. N. – Kotova, O. B. – Silaev, V. I. – Rostovtsev, V. I. – Kiseleva, D. V. – Kondraťev, S. A.: Microphase Heterogenization of High-Iron Bauxite as a Result of Thermal Radiation, Journal of Mining Science, Vol. 55. No. 5 (2019) 811–823 p. https://link.springer.com/content/pdf/10.1134/S1062739119056185.pdf

[3] Kurovics, Emese – Kotova, Olga B. – Gömze, László A .– Shushkov, Dmitry A. – Ignatiev, Grigoriy V. – Sitnikov, Petr A. – Ryabkov, Yuri I. – Vaseneva, Irina N. – Gömze, Ludmila N.: Preparation of particle-reinforced mullite composite ceramic materials using kaolin and IG-017 bio-origin additives Építőanyag – JSBCM, Vol. 71, No. 4 (2019), 114–119. p. https://doi.org/10.14382/epitoanyag-jsbcm.2019.20

[4] Kotova, O et al 2018 Proceedings of the 10th Edition of Euroinvent European exhibition of creativity and innovation. Euroinvent . 10-31 Mai 2018 "George Enescu", Iasi, Romania 550. p.

[5] Ponaryadov, A. – Kotova, O.: Phosphate sorption on leucoxene, Vestnik of Geosciences No. 1 (2020) 19–23. p. https://doi.org/10.19110/geov.2020.1.3

[6] Tatlock, D. B.: Rapid modal analysis of some felsic rocks from calibrated X-ray diffraction patterns: U.S. Geol. Survey Bull. 1209 (1966) 41. p.

[7] Andrews, J. T. – Kristjansdottir, G. B. – Eberl, D. D. – Jennings, A.: A quantitative X-ray diffraction inventory of the tephra and volcanic glass inputs into the Holocene marine sediment archives off Iceland: A contribution to V.A.S.T., Polar Research, Vol. 32. (2013) https://doi.org/10.3402/polar.v32i0.11130

[8] Wadsworth, W. B. – Baird, A. K.: Modal analysis of granitic rocks by X-ray diffraction, Canadian Mineralogist Vol. 27 (1989) 323-341. p. https://pdfs.semanticscholar.org/4891/94475f823737a1cbba85a4d77b51f2537048.pdf

[9] Zhao, P. – Lu, L. – Liu, X. – De la Torre, A.G. – Cheng, X.: Error Analysis and Correction for Quantitative Phase Analysis Based on Rietveld-Internal Standard Method: Whether the Minor Phases Can Be Ignored? Crystals Vol. 8 No. 3. (2018) 110. p. https://doi.org/10.3390/cryst8030110

[10] Piip, B.I., 1946. A new flank crater on Plosky Tolbachik Volcano. Bull. Vol. Obs. Kamchatka Vol. 13 (1946) 10–21. p.

[11] Fedotov, S.A.: The 1975–1976 Large Tolbachik Fissure Eruption in Kamchatka, Moscow, Nauka, (1984) 637. p.

[12] Churikova, T. G. – Gordeychik, B. N. – Iwamori, H. – Nakamura, H. – Ishizuka, O. – Nishizawa, T. – Haraguchi, T. – Miyazaki, T. – Vaglarov, B. S.: Petrological and geochemical evolution of the Tolbachik volcanic massif, Kamchatka, Russia, J. of Volcanology and Geothermal Research Vol. 307 No. 1 (2015) 156-181. p. https://doi.org/10.1016/j.jvolgeores.2015.10.026

[13] Corsaro, R.A. – Miraglia, L. – Pompilio, M.: Petrologic evidence of a complex plumbing system feeding the July–August 2001 eruption of Mt. Etna, Sicily, Italy. Bull Volcanol Vol. 69. (2007) 401-421. p. https://doi.org/10.1007/s00445-006-0083-4

Electroacoustic properties of quartz minerals in a finely dispersed state

Leonid N. Kotov ▪ Syktyvkar State University, Syktyvkar, Russia ▪ kotovln@mail.ru
Elena L. Kotova ▪ Saint-Petersburg Mining University, Russia ▪ kotova_el@pers.spmi.ru
Ludmila N. Gömze ▪ IGREX Engineering Service Ltd, Hungary ▪ igrex@freemail.hu

Leonid N. KOTOV
is a Prof., Head of Radioelectronics Department, Syktyvkar state University, Russia, author of 392 scientific papers.

Elena L. KOTOVA
is a Scientific Director of the Mining Museum of the Saint-Petersburg Mining University. Author and co-author of chapter in book, patent and more than 30 articles. The member of the Russian Mineralogical Society, Oil and Gas Historical Society of Russia

Ludmila N. GÖMZE
is MSc (civil engineer), managing director of the IGREX Engineering Ltd. Author or co-author more than 30 scientific papers. She is one of the main organizers of the 2nd European Conference on Silicon and Silica Based Materials (www.ec-siliconf.eu)

Abstract

The authors described a new method for studying the electroacoustic properties of piezoelectric particles and substances in a finely dispersed state. They obtained the values of the quality factor and the amplitude of electro-elastic vibrations of piezoelectric quartz particles with an average size of 75 microns. To observe the high-frequency response, the generator excited quartz powders with a pulsed electric field with a frequency of 16.5 MHz. The characteristics and quality factor of electro-elastic vibrations of powder particles of the following types of quartz were determined: artificial, smoky, citrine, amethyst, re-crystallized, veined granular, veined pole-shaped. The content of impurities in the minerals of quartz is given. The presence of aluminum ions Al^{3+} in quartz minerals also causes a strong increase in the quality factor of electro-elastic vibrations of piezoelectric particles, which may also be associated which may be associated with a change in the surface charge of quartz particles. The authors also carried out studies on the distribution of quality factor and response amplitudes electro-elastic vibrations over regions of a large citrine plate.

Keywords: electroacoustic properties, quality factor of electro-elastic vibrations, minerals of quartz, piezoelectric particles, powder

Kulcsszavak: elektroakusztikus tulajdonságok, az elektro-elasztikus rezgések minőségi tényezője, kvarc ásványai, piezoelektromos részecskék, por

1. Introduction

Piezoelectric materials are important functional materials that can generate an electrical response when the deformation of a solid with time changes [1-3]. Among the many different types of piezoelectric materials, quartz crystals are one of the most widely used traditional piezoelectric materials [4]. Piezoelectric materials are essential parts of the electronics and electrical equipment used for consumer and industrial applications, such as ultrasonic piezoelectric transducers, resonators, sensors, actuators, transformers. The development and use of elements and devices of functional electronics is currently an important and rapidly developing field of technology [5-9]. A distinctive feature of functional electronics is the performance of operations on radio signals in the absence of traditional discrete elements: capacitors, resistances, transistors, etc. Radio signals are processed as a result of the interaction of electromagnetic radiation with the special physical properties of a solid medium, for example, the elastic properties in which this radiation propagates. Functional acoustoelectronics occupied a special place among these areas, which had already found wide practical application due to its great technical capabilities. Widely used elements of acoustoelectronics, such as resonators on surface acoustic waves in cell phones. In acoustoelectronics, the excitation of acoustic vibrations and waves is widely used when a solid is placed in a high-frequency electromagnetic field.

Measurement of acoustic parameters, such as piezoelectric constants, Q-factor of oscillations of a piezoelectric solids, signal saturation field amplitude have become the most sensitive methods, and sometimes the only possible methods

for determining the nature of materials [10-12]. One of the most important properties of quartz crystals is the infinitesimal damping of elastic vibrations or the infinitely large Q-factor of vibrations. Therefore, most effective devices of functional acoustoelectronics are built using a wide class of single crystals with various physical properties. A wide variety of physical properties is provided by nature, which under natural conditions has created many different crystals that cannot yet be created artificially [13]. In research work [14] the mechanisms of enhancing the piezoelectric properties and increasing the quality factor of vibrations by introducing impurities during the growth of quartz minerals in natural conditions was examined. This paper presents the results of a study of the acoustoelectronic properties and the quality factor of electro-elastic vibrations of the quartz minerals in comparison with similar properties of artificial quartz grown by man.

2. Experimental methods and technique

The electroacoustic response (EAR) method can be a convenient method to study electrical and elastic properties of crystals in a finely dispersed state (particles and powders) [10,12]. EAR method consists in the formation of an electric signal after excitation of a set of crystalline piezoelectric particles (piezoelectric powder) by electric impulse. EAR method allows studying dynamic electrical and elastic characteristics of substance at large amplitudes of electric fields and elastic deformations, which are unattainable by other methods. This method is simpler than the well-known electro-acoustic echo method, since it uses one radio frequency pulse

No.	Type of quartz	Content of impurity elements, 10^4 wt %								
	elements	Al	Ti	K	Mg	Na	Fe	Li	Cu	Mn
2	Smoky	32.4	17.1	18.8	3.8	3.9	5.4	0.6	0.6	0.2
3	citrine	222	13.1	7.5	1.7	2.5	no	19.2	0.5	0.1
4	amethyst	27.3	4.5	2.6	1.2	1.9	no	4.1	0.9	0.1
5	vein recrystallized	51	16.3	4.5	4.7	9.9	no	4.5	0.5	0.2
6	vein granular	384	24.2	27	25	21.5	19.5	0.08	1.3	0.5
7	vein columnar	79	21.8	23.1	8.5	30	5.8	0.2	0.4	0.2

1. táblázat   A kvarc ásványok szennyeződései
Table 1   Content of impurities in the minerals of quartz.

to excite powder particles [10, 12]. A close two-pulse echo technique involves exposing the powder to two pulses. For the effective excitation of elastic vibrations of piezoelectric particles, it is necessary that the condition of acoustic resonance is satisfied, that is, when the particle sizes are of the order of the elastic wavelength. With its help, it is possible to study charges, defects, and their mobility in crystalline particles, which appear in large samples only in a weak form. The analysis of results of study of substance by EER method is possible only with a clear understanding of the mechanisms resulting in formation of a high-frequency response and time intervals of observing the electrical response. To clarify the differences in the electro-elastic properties of various quartz minerals, piezoelectric powders made from artificial and quartz minerals (α-SiO$_2$) with different content of impurities created under natural conditions were used.

The electro-elastic response can be observed in powders in time intervals during which sound attenuation in the crystal occurs [11]. This time for solids does not exceed a fraction of a second, therefore, the existing standard equipment for observing nuclear-quadrupole resonance (NQR) satisfies all the requirements imposed on the duration, amplitude of radio frequency pulses, and amplitude of weak receiving signals. In this work, all studies of the electroacoustic response of quartz powders on a pulsed panoramic spectrometer (ISP-1, USSR) were performed. The main blocks and elements are (*Fig. 1*): RF pulse generator, matching and measuring device in the form of LC circuit (inductance coil with capacitor), HF receiver of weak signals, an oscilloscope for observing signals. The spectrometer ISP-1 had the following characteristics: operating frequency range 1–20 MHz, duration of radio pulses 1–100 μs, amplitude of voltage supplied to a capacitor with inductor 0.1–3 kV. Dead time interval is from the end of the exciting pulse at which it is impossible to observe the electro-elastic response, was 30 μs. All measurements were performed at room temperature. During the experiments amplitude of the electric response at a frequency 16.5 MHz after time τ=30 μs from an exciting radio frequency (RF) pulse with a duration $\Delta t = 4$ μs were determined. The quality factor of electro-elastic vibrations of the particles of quartz powder $Q = N$, where N is the number of vibrations for which the response amplitude decreases in e times.
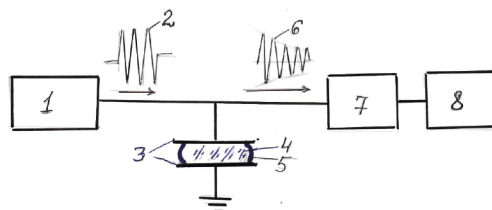
1. ábra   A piezoelektromos porok elektro-elasztikus válaszának vizsgálatára szolgáló berendezés vázlata. Az ábrán látható: 1 - rádiófrekvencia-generátor, 2 - rádiófrekvencia-impulzus, 3 - kondenzátorlemezek, 4 - kvarcpor, 5 - ampulla, 6 - elektromos válasz, 7 - rádiófrekvenciás vevő, 8-oszcilloszkóp.
Fig. 1   The block diagram of the installation for the study of electro-elastic response from piezoelectric powders. The diagram shows: 1 - a radio frequency generator, 2 - a radio frequency pulse, 3 - capacitor plates, 4 - quartz powder, 5 - an ampoule, 6 – electrical response, 7 - a radio frequency receiver, 8-oscilloscope.

3. Preparation, characteristics and composition of samples

The experiments on the study of quartz were performed on powder samples placed in glass ampoules with a diameter of 0.6 cm and a length of 2 cm [12]. The volume of quartz powder in all experiments was 0.3 cm^3. After high-temperature heating at 700 K and pumping air from the ampoules to pressure 10^2 Pa, the ampoules were sealed. Vacuum of the powder was done in order to reduce the attenuation of the elastic vibrations of the powder particles by air molecules and to prevent the adsorption of air molecules, especially oxygen molecules and OH hydroxyl groups, on the surface of quartz particles [12]. For effective radio-frequency excitation and observation of the electro-elastic response of powder particles, it is necessary that the dimensions of the excited powder particles l_i correspond to the condition of elastic resonance, and the length of the elastic half-wave in the test substance to be equal to , where – length, speed and frequency of an elastic wave [11]. Considering that in the experiments: ν = 16.5 MHz, $\vartheta \approx 5.75 \cdot 10^3$ m·s^{-1}, the particle size of all the studied quartz powders was $l_i \approx (50 \div 100)$ μm.

In the Subpolar Urals (Russia), a wide variety of vein quartz is widely developed, which is used as technical raw material. *Table 1* shows average content of impurities of hydrothermal vein quartz of the Lyapinsky anticlinorium [15, 16]. The content of impurities (Al, Cu, Fe, Mg, Mn) was determined by the spectral method at the Institute of Geology of the Komi Science Center of the Ural Branch of the Russian Academy of Sciences (Syktyvkar, Russia), Na, Ka, Li – at St. Petersburg Mining University (St. Petersburg, Russia).
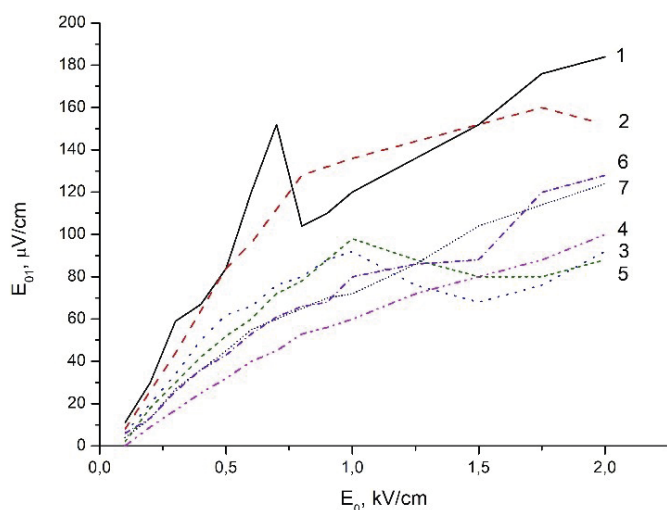
No.	Types of quartz	Q·10⁻³	E_{01}, µV/cm	E0max, kV/cm
1	artificial	9,2	120	0.7
2	smoky	38,1	96	0.8
3	citrine	43,1	66	0.7
4	amethyst	11,6	40	0.8
5	vein recrystallized	20,0	60	0.8
6	vein granular	16,5	55	0.6
7	vein columnar	7,1	53	0.6

2. táblázat   A kvarc ásványi porok elektroakusztikus reakcióinak jellemzői
Table 2   Characteristics of the electroacoustic responses of quartz mineral powders.

4. Results and discussion

In this paper for the first time is presented data on the study of the electroacoustic properties of various types of quartz minerals by the method (*Table 2*) [17, 18]. The table shows the following values: Q - quality factor of electro-elastic vibrations; E_{01}-response amplitudes after exposure to one pulse; E_{0max} - the amplitude of the electric field at which the saturation of the amplitude of the elastic vibrations of the particles begins. Amplitudes E_{01} were recorded on an oscilloscope at time τ= 30 µs after the action of an pulse of duration *4 µs* with amplitude E_0 = 0.6 kV/cm.

As can be seen from the table, the piezoelectric effect is most pronounced for artificial and smoky quartz (the response amplitude E_{01} is proportional to the piezoelectric moduli). Amethyst quartz has the weakest high-frequency piezoelectric effect among minerals. The large value of Q factor of electro-elastic vibrations of powder particles is characteristic of citrine quartz, which is most likely due to the high content of aluminum impurities in it (*Table 1*), which results in decreasing sound attenuation, since $Q \sim \alpha^{-1}$, α – sound attenuation coefficient [11]. Small values of the quality factor Q of oscillations correspond to artificial and columnar quartz. Small values may be associated with a low content of aluminum impurities.

Dependences of the response amplitude on the field amplitude were divided into two areas (*Fig. 2*). For the first region at $E_0 < E_{0max}$, a linear increase in the response amplitude from the amplitude of the electric field is observed. The second region $E_0 > E_{0max}$ corresponds to the saturation region of the elastic vibrations of the quartz powder particles. For most quartz, especially artificial quartz, the jumps in the response amplitude were observed in the saturation region. Perhaps this is due to the presence of HF breakdown in quartz particles.

Studies on the distribution of quality factor and response amplitudes electro-elastic vibrations over regions of a citrine polished plate with dimensions 275·122 mm² and thickness 4 mm (*Fig. 3*) were also carried out. This plate is made of a large mineral. In the center of the citrine plate, the response amplitudes are E_{01} = 90, and at the edges less than $E_{01} \approx 60$, which corresponds to the fact that the crystallinity at the center of quartz minerals is better than at the edges. The quality factor is $Q \approx 28 \cdot 10^3$ in the center of the citrine plate, and more than $Q = 15 \cdot 10^3$ at the edges, which corresponds to the fact that the amount of impurities, especially *Al*, is much larger at the edges than in the center. The largest values of the amplitude of the electro-elastic response E_{01} correspond to the two central cells of the mineral plate. It was hypothesized that the central regions of the mineral have a good degree of crystallinity.

2. ábra   A válasz amplitúdójának függése a kvarcok HF mező amplitúdójától: mesterséges (1), füstös (2), citrin (3), ametiszt (4), erezetten átkristályosodott (5), erezett-szemcsézésű (6), oszlopos erezetű (7)

Fig. 2   Dependences of the response amplitude on the HF field amplitude for quartz types: artificial (1), smoky (2), citrine (3), amethyst (4), vein recrystallized (5), vein granular (6), vein columnar (7)

3. ábra   Az E01 (a számlálóban) és a Q-tényező (a nevezőben 10-3-kal szorozott) amplitúdójának eloszlása az elektro-elasztikus rezgésekkel a citrinlemez celláiban

Fig. 3   Distribution of response amplitudes E_{01} (in the numerator) and Q-factor (multiplied by 10⁻³ in the denominator) electro-elastic vibrations in the cells of a citrine plate.

5. Conclusions

A new method was described for studying the electroacoustic properties of piezoelectric particles and substances in a finely dispersed state. The values of the quality factor Q and the amplitude of electro-elastic vibrations of quartz particles with an average size of 75 microns were obtained. Quartz minerals from the hydrothermal veins of the Lyapinsky anticlinorium (Subpolar Ural, Russia) were investigated. The content of impurities in the minerals of quartz is given. The characteristics and quality factor of electro-elastic vibrations of powder particles of the following types of quartz were determined: artificial, smoky, citrine, amethyst, re-crystallized, veined granular, veined pole-shaped. The results have shown that the qualitative factor of electro-elastic vibrations is determined by the state of the surface and the presence of water in quartz particles. For example, vacuum heat treatment (at 600 K) of the surface of a quartz piezoelectric powder results in increasing quality factor of particle elastic oscillations by more than an order of magnitude. Such an increase in the quality factor of vibrations is associated with the physical and chemical desorption of molecules from the surface of piezoelectric particles during vacuum heat treatment. The breaking of bonds on the surface of quartz particles due to desorbed molecules increases the need for compensation of electric fields and results in the redistribution of charges in the particles. From this fact can be concluded that the presence of a surface charge on particles creates a state like a stretched string. The presence of aluminum ions Al^{+3} in quartz minerals also causes a strong increase in the quality factor of electro-elastic vibrations of piezoelectric particles, which may also be associated with this state. Studies on the distribution of quality factor and response amplitudes electro-elastic vibrations over regions of a citrine polished plate were also carried out.

Acknowledgment

References

[1] Zhang, S. – Li, F. – Yu, F. – Jiang, X – Lee, H. Y. – Luo, J. –Shrout, T. R.: Recent Developments in Piezoelectric Crystals. Review. Journal of the Korean Ceramic Society, Vol. 55 No. 5 (2018) 419-439. p. https://doi.org/10.4191/kcers.2018.55.5.12

[2] Heywang, W. – Lubitz, K. – Wersing, W.: Piezoelectricity: Evolution and Future of a Technology. NY: Springer Science & Business Media (2008)

[3] Li, F. – Cabral, M. J. – Xu, B. – Cheng, Z. X. – Dickey E. C. at al.: Recent developments in piezoelectric crystals. J. Korean Ceram. Soc., Vol. 55 (2018) 419–439. p.

[4] Mohammadi, M. M.: A comparison between quartz and PZT ceramic for Sensoric applications. Research Desk. Vol. 2 No. 4. (2015)

[5] Park, S. E. – Shrout, T.R.: Ultrahigh strain and piezoelectric behavior in relaxor based ferroelectric single crystals. J. Appl. Phys. Vol. 82 (1997) 1804–1811. p.

[6] Trolier-McKinstry, S. –Zhang, S. –Bell, A. J. – Tan. X.: High-Performance Piezoelectric Crystals, Ceramics, and Films. Annu. Rev. Mater. Res., Vol. 48 No. 1. (2018) 191–217. p.

[7] Iwazaki, Y. – Yokoyama, T. – Nishihara, T. – Ueda, M.: Highly enhanced piezoelectric property of co-doped AlN. Appl. Phys. Express, Vol. 8 (2015) 061501.

[8] Hackenberger –Bellaiche, L. –Xu, Z. –Chen, L. Q. –Shrout, T. R. –Zhang, S. J.: Giant piezoelectricity of Sm-doped Pb (Mg1/3Nb2/3)O3–PbTiO3 single crystals. Science, Vol. 364 (2019) 264–268. p.

[9] Moreira, M. – Bjurström, J. – Katardjev, I. – Yantchev, V.: Aluminum scandium nitride thin- film bulk acoustic resonators for wide band applications. Vacuum, Vol 86 (2011) 23-26. p.

[10] Kajimura, K.: Dynamic polarization echoes in powders materials. In: Phys. Acoust., N.Y., Vol. 16 (1982) 295-340. p.

[11] Ultrasound. Little Encyclopedia. Editor-in-chief Golyamina I.P. Soviet Encyclopedia. Moscow, (1979) 400 p.

[12] Shutilov, V. A. – Andzhikovich, I. E. – Komashnya, V. L. – Kotov, L. N.: Glass-like anomalies of electro-acoustic echo in crystalline quartz powders. Solid State Physics, Vol. 27 No. 3 (1985) 929-930. p.

[13] Kurovics, E. – Kotova, O. B. – Gömze, L. A .– Shushkov, D. A. – Ignatiev, G. V. – Sitnikov, P. A. – Ryabkov, Y. I. – Vaseneva, I. N. – Gömze, L. N.: Preparation of particle-reinforced mullite composite ceramic materials using kaolin and IG-017 bio-origin additives, Építőanyag – JSBCM, Vol. 71, No. 4 (2019), 114–119. p. https://doi.org/10.14382/epitoanyag-jsbcm.2019.20

[14] Kotova, O. B. – Harja, M. – Kotov L. N. – Ponaryadov, A. V.: Titanium minerals as prototypes of functional materials with pronounced electromagnetic properties // Vestnik of Institute of Geology of Komi SC of UB of RAS. No. 4. (2018) 34–39. p. (doi 10.19110/2221-1381-2018-4-34-39)

[15] Kuznetsov, S. K.: Vein quartz of the circumpolar Urals. St. Petersburg: Nauka, (1998) 204 p.

[16] Lyutoev, V. P.: Chalcedony structure and spectroscopy. UB RAS, Yekaterinburg, (2004) 116 p.

[17] Kotov, L. N. – Yukhtanov P.P.: Mechanisms of attenuation of electro-acoustic echo. Collection of materials of the conference "Structure, substance, history of the lithosphere of Timan-Northern Ural segment". Syktyvkar, (1992) 62.

[18] Kotov, L. N. Electroacoustic echo in quartz powders. Theses of the All-Union Conference "Mineralogy of quartz". Syktyvkar, (1992) 32.

TURKEYTRIB 2020 3rd INTERNATIONAL CONFERENCE ON TRIBOLOGY

June 18-20 2020

~~POSTPONED TO DECEMBER 2020~~

CONFERENCE VENUE: Elite World Prestige Hotel
ADDRESS: Şehit Muhtar Caddesi No:40, 34435 Taksim Istanbul-TURKEY
WELCOME TO TURKEYTRIB 2020!

We are very pleased to announce that the 3rd International Conference on Tribology TURKEYTRIB 2020 will be held from 18 to 20 June 2020 at the Elite World Prestige Hotel Taksim-İstanbul-TURKEY. The scope of this conference embraces the state of art and future trends in tribology research and application, emphasizing the necessity of facilitation intellectual collaboration across both disciplinary and national-international boundaries. The main objective of the conference is to provide a unique opportunity of presenting and discussing recent developments in different aspects of Tribology and strengthen the linkage between academia and industry. The conference consists of scientific sessions, symposia on specific topics, exhibitions and various collateral events. Turkish and Foreign groups of experts will have chance to share information and get in touch with other groups in all part of Tribology. Nowadays these aspects are becoming more and more important both in respect of human life and environment.
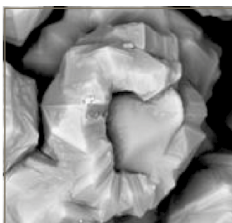
– SPECIAL ISSUE (Web of Science Core Collection-Emerging Sources Citation Index): Selected high-quality papers (10) presented at the TurkeyTrib'20 conference will be selected and invited to submit their contributions for Special Issue publication in Építőanyag - Journal of Silicate Based and Composite Materials. (SCIE; Impact Factor 1.079 (2018). The submission due is 30 June 2020.

www.turkeytribconference.com/index.php/en/

We are pleased to announce the organization of

ic-cmtp6
THE 6TH INTERNATIONAL CONFERENCE
ON COMPETITIVE MATERIALS AND TECHNOLOGY PROCESSES
to be held in Hotel Palota in Miskolc-Lillafüred in May 3-7, 2021

The **ic-cmtp6** conference will be held in the wonderful palace of **Hotel Palota** in the exceptionally beautiful environment of **Beech Mountain** in **Miskolc-Lillafüred** in **Hungary**. In 2018 in the previous conference scientists had participated from **46** countries of **5** continents and the largest delegations have arrived from **Japan, Russian Federation, China, Czech Republic,** and **Korea**.

THE CONFERENCE SESSIONS

1. Advanced Ceramics and Nanoceramics
2. Advanced Composites and Nanocomposites
3. Advanced Materials for Bio- and Medical Applications
4. Advanced Materials for Extreme Applications
5. Advanced Nanomaterials and Nanocomposites
6. Advanced Optical Materials – Properties and Applications
7. Advanced Polymer-Clay Nanocomposites
8. Advanced Powder Metallurgy Materials
9. Advanced Processing and Characterization Methods for Nanocomposites
10. Bioelectronic Materials and Biosensors
11. Biomaterials Derived Ceramics and Nanocomposites
12. Clay Minerals and Organo-Clay Complexes
13. CO2 Capture and Fixing Materials and Methods
14. Glasses and Related Competitive Materials
15. Graphene – Properties and Applications
16. Hetero-Modulus and Hybrid Materials
17. Intelligence and Smart Materials – Structures, Properties and Applications
18. Interface as a Functional Material – Behavior, Function and Application
19. Light Weight Materials with Predesigned and Controlled Nanostructur
20. Materials and Methods to Capture and Fixing Radioactive Pollutants from Waters and Soils
21. Materials for Membranes and Catalysts
22. Materials for Biological Systems and Health
23. Materials for Energy Saving and Conservation
24. Materials for Harvesting Renewable Energy
25. Materials for Sensors and Actuators
26. Materials with Extreme Dynamic Strength
27. Mechanical Properties and Processing Technology of Advanced Materials
28. Minerals for Environmental and Medical Application
29. Nanomaterials Applied to Biomedical Applications and Nanomedicine
30. Nanomaterials for Electronic and Electrotechnical Applications
31. Novel Synthesis and Processing Technology
32. Polymer Derived Ceramics and Advanced Nanocomposites
33. Processing and Properties of Silicate Ceramics
34. Sol-Gel Technology in Materials Processing
35. Testing and Characterization of Materials – Methods, Equipment and Uncertainties
36. Traditional Ceramics and Building Materials
37. Traditional Ferrous and Nonferrous Metals

In case of pandemic quarantine of COVID-19 or other force majeure situation the conference ic-cmtp6 will be held in the same place in October 4-8, 2021.

Registration and further information: www.ic-cmtp6.eu